Influence of the electrolyte on the electrode reactions in the chlorate process

Linda Nylén

KTH Chemical Science and Engineering

Doctoral thesis
KTH – Chemical Science and Engineering
Department of Chemical Engineering and Technology
Applied Electrochemistry
SE-100 44 Stockholm, Sweden

TRITA-CHE-Report 2008:22

ISSN 1654-1081

ISBN 978-91-7178-918-1

Akademisk avhandling som med tillstånd av Kungliga Tekniska Högskolan i Stockholm framlägges till offentlig granskning för avläggande av teknologie doktorsexamen fredagen den 18:e april 2008 kl 10.00 i V2, Kungliga Tekniska Högskolan, Teknikringen 76, Stockholm

ABSTRACT

The chlorate process is very energy intensive and a major part of the production costs are for electrical energy. Since the electricity prices are constantly increasing and may also vary periodically, the chlorate plants may be forced to adjust their production rate to the price at each moment in order to minimise their costs. Variation of current load requires increased knowledge regarding the electrode behaviour in a wide current range. In this thesis, the aim was to study the impact of the electrolyte on the electrode reactions in order to reduce the energy consumption. The work has mainly been experimental and additionally mathematical modelling has been carried out. A wide current range has been investigated in order to increase the understanding of the phenomena and to obtain results useful for low-load operation during the periods of high electricity cost.

To operate the anode as energy efficiently as possible, the anode potential should not exceed the critical potential (E_{cr}), where the slope of the anodic polarisation curve increases, most likely due to ruthenium(VIII)-formation, and where the side reaction of oxygen evolution increases. In this work, the influence of different electrolyte parameters on E_{cr} has been studied. It was shown that a higher chloride concentration and an increased temperature lowered E_{cr}, which was expected to increase the risk of exceeding E_{cr}. However, this was not observed due to a simultaneous favouring of the chloride oxidation. Hence it was concluded that the electrolyte parameters should be optimised so that the lowest possible anode potential is obtained, which would enable higher current densities without exceeding E_{cr}. A further conclusion is that the increased slope of the polarisation curve at E_{cr} was possibly related to the lower activity for chloride oxidation on ruthenium oxidised to ruthenium(VIII).

At full-load operation, the cathode potential was shown to be rather independent of the electrolyte composition despite a large variation of electrolyte parameters. The cathode composition appears to be more critical than the electrolyte composition when aiming at reducing the energy consumption. A strategy to increase the cathode activity could be to in situ apply a catalytic film onto the electrode surface. Therefore, Y(III) was added to a chloride electrolyte in order to form a yttrium hydroxide film on the alkaline cathode surface during hydrogen evolution. The yttrium-hydroxide film activated reduction of water (hydrogen evolution) and hindered hypochlorite reduction, proton reduction and nitrate reduction. The inhibiting properties are important for the prevention of side reactions, which currently are avoided by reducing Cr(VI) of the electrolyte on the cathode, producing an inhibiting chromium-hydroxide film. The studies on Y(III) increase the expectations for finding alternatives to the toxic Cr(VI).

The addition of chromate to the chlorate electrolyte gives a high cathodic current efficiency and chromate has buffering properties in the electrolyte. The role of the buffer has been investigated for the oxygen evolution from water (one possible anodic side reaction), as well as cathodic hydrogen evolution. Models have been developed for these systems to increase the understanding of the interaction between buffer, electrode reactions and mass transport; the results have been verified experimentally. The chromate buffer increased the limiting current significantly for the cathodic H^+ reduction and the cathodic overpotential was reduced drastically at currents lower than the limited current. A too low overpotential could result in the cathodic protection being lost. The presence of chromate buffer increased the limiting current for the oxygen evolution from OH^-. The modelling of these systems revealed that the homogeneous reactions connected to the electrode reactions were not in equilibrium at the electrode surface. Further, a good resolution of the interface at the electrode surface was crucial since the, for the electrode reactions, important buffering takes place in an nm-thick reaction layer.

Keywords: Chlorate, chloride oxidation, critical anode potential, chromate, DSA, hydrogen evolution, iron, mass transport, oxygen evolution, REM, RDE, steel

SAMMANFATTNING

Framställning av klorat är mycket energiintensiv och kräver stora mängder elenergi. Stigande elpriser, som dessutom ofta varierar under dygnet eller säsongsvis, gör att man vill reducera onödiga förluster samt ibland försöka anpassa produktionen så att man när elpriset är högt minskar den, för att sedan öka produktionen igen då elpriset sjunker. Denna flexibla drift kräver ny kunskap om hur elektroderna beter sig i ett större strömintervall än vad som tidigare varit av intresse. Målet med detta arbete var att, med fokus på elektrolytens betydelse, identifiera möjliga förbättringar för kloratprocessen och därmed minska energiförbrukningen. Studierna har i huvudsak varit experimentella men även matematisk modellering har använts. Ett brett strömintervall har undersökts för att bättre förstå fenomenen och för att även kunna använda resultaten då höga elpriser gör att man vill köra processen vid lägre laster än normalt.

För att driften av anoden ska vara så energieffektiv som möjligt bör anodpotentialen inte överskrida den kritiska potentialen (E_{cr}), där den anodiska polarisationskurvan får en högre lutning (troligtvis pga Ru(VIII)-bildning) och bireaktionen syrgasutveckling ökar. I detta arbete har påverkan av olika elektrolytparametrar på E_{cr} undersökts. Det visade sig att en ökad kloridkoncentration och ökad temperatur sänkte E_{cr}. Trots att detta borde göra att E_{cr} lättare överskrids, blev inte detta fallet eftersom kloridoxidationen samtidigt gynnades. Slutsatsen blir därför att elektrolytparametrarna bör optimeras så att lägsta möjliga anodpotential uppnås, vilket då även gör att strömtätheten kan ökas utan att E_{cr} överskrids. Slutsatsen är vidare att polarisationskurvans högre lutning vid E_{cr} kan ha att göra med att rutenium oxiderat till rutenium(VIII) har lägre aktivitet för kloridoxidation.

Vid full last visade sig katodens potential vara relativt oberoende av elektrolytsammansättningen trots att denna varierades kraftigt. Katodens sammansättning verkar vara viktigare att ta hänsyn till än elektrolytens för kunna åstadkomma en större energibesparing. Ett alternativ till att öka katodens aktivitet skulle vara att in-situ belägga elektrodytan med en katalytisk film. Försök gjordes att sätta till Y(III) till kloridelektrolyt för att under vätgasutveckling fälla ut en yttriumhydroxidfilm på den alkaliska katodytan. Yttriumhydroxidfilmen aktiverade vattenreduktion (vätgasutveckling) och inhiberade hypokloritreduktion, protonreduktion och nitratreduktion. De inhiberande egenskaperna är viktiga för att förhindra bireaktioner, vilka idag hindras av att Cr(VI) i elektrolyten reduceras på katoden och bildar en hindrande kromhydroxidfilm. Försöken med Y(III) visar att det finns goda möjligheter att hitta alternativ till det miljöfarliga Cr(VI).

Kromattillsatsen i kloratelektrolyt ger förutom ett högt katodiskt strömutbyte även en buffrande effekt till elektrolyten. Effekten av buffert har undersökts för en av de anodiska bireaktionerna, syrgasutveckling ur vatten, samt för vätgasutvecklingen på katoden. Dessa system har modellerats för att bättre förstå samspelet mellan buffert, elektrodreaktioner och materietransport och resultaten har verifierats experimentellt. Kromatbufferten ökade gränsströmmen för katodisk H^+-reduktion betydligt och katodöverpotentialen sjönk kraftigt vid lägre strömmar än gränsströmmen. Detta kan vara ett problem om överpotentialen sjunker så lågt att elektroden inte är katodiskt skyddad. För syrgasutvecklingen ökade närvaron av kromatbuffert gränsströmmen för syrgasutveckling ur OH^-. Modellering av dessa system visar att de homogena reaktioner som var kopplade till elektrodreaktionerna inte var i jämvikt vid elektrodytan. Vidare visade det sig vara mycket viktigt med en bra upplösning av gränsskiktet vid elektrodytan, då den buffring som är viktig för elektrodreaktionerna sker i ett mycket tunt reaktionsskikt (nanometertjockt).

Nyckelord: DSA, järn, Klorat, kromat, kloridoxidation, kritisk anodpotential, materietransport, RDE, stål, REM, syrgasutveckling, vätgasutveckling

LIST OF PAPERS

The thesis is a summary of the following papers:

I. **Investigation of the oxygen evolving electrode in pH Neutral Electrolytes. Modelling and experiments of the RDE cell**
L. Nylén, M. Behm, A. Cornell and G. Lindbergh
Electrochim. Acta, **52**, 4513 (2007)

II. **Critical Anode Potential in the Chlorate Process**
L. Nylén and A. Cornell
J. Electrochem. Soc., **153**, D14 (2006)

III. **Effects of electrolyte parameters on the chlorate cathode potential**
L. Nylén and A. Cornell
Submitted to *J. Appl. Electrochem.*

IV. **Cathodic reactions on an iron RDE in the presence of Y(III)**
L. Nylén, J. Gustavsson and A. Cornell
Submitted to *J. Electrochem. Soc.*

TABLE OF CONTENTS

1. INTRODUCTION

In this chapter a short introduction to the chlorate process is given. It is not intended to be exhaustive, but rather aims to illustrate the width of the subject and to give a background for the studies in the thesis.

Chlorate is today mostly produced in the form of sodium chlorate ($NaClO_3$). It is the raw material in production of chlorine dioxide (ClO_2), commonly used in pulp bleaching [1]. In Sweden, Eka Chemicals (Akzo Nobel) is the only chlorate manufacturer, and has plants in Stockvik/Sundsvall and Alby. The development of electrochemical chlorate production in Sweden was induced by the need for potassium chlorate ($KClO_3$) in the 1880's when the manufacturing of a Swedish invention, the safety match, required large amounts of $KClO_3$. Nowadays, a very small part of the chlorate produced serves as raw material for matches, and the pulp industry is consuming most of the chlorate.

The total production capacity of the chlorate plants world-wide was 2005 around 3 million tonnes sodium chlorate, and the actual amount of chlorate produced will probably be close to that figure [2]. The countries with largest production are shown in Figure 1. Canada and US the largest producers and together contribute approximately 60 % of all sodium chlorate.

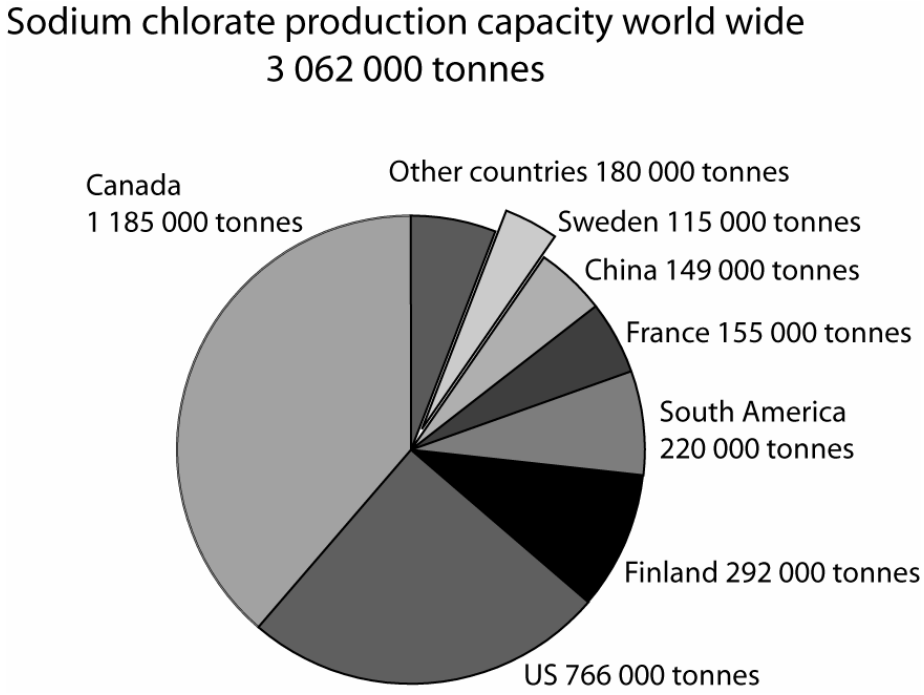

Figure 1. World-wide production capacity of sodium chlorate in 2005 [2].

The chlorate process consumes significant amounts of electrical energy. In fact, electrical energy constitutes up to 70 % of the production costs [2]. Due to high energy consumption and large production volumes even a small efficiency improvement may save large amounts of energy.

With increasing electricity prices it becomes even more important for the chlorate producers to operate their plants so that their energy costs are minimised. It may be done by reducing the energy losses and by varying the production rate so that it is low when electricity prices are high. The demand for operating at varying current load requires knowledge about how the electrodes behave in a wide current-density range. For instance, when operating at low current load it has to be ensured that the cathode is under cathodic protection to avoid corrosion.

1.1 Chlorate chemistry

Chlorate is produced in undivided cells, where the overall reaction (reaction 1) is sodium chloride and water forming sodium chlorate and hydrogen. A typical chlorate electrolyte consists of about 500-650 g/L sodium chlorate ($NaClO_3$), 80-120 g/L sodium chloride (NaCl), 2-6 g/L sodium hypochlorite (NaClO) and Cr(VI) added as 3-8 g/L sodium dichromate ($Na_2Cr_2O_7$); the electrolyte has a pH of 6-7 and a temperature of 70-80 °C. The most common electrodes are ruthenium-based dimensionally stable anodes (DSAs) and cathodes of steel.

The hydrogen bubbles formed in the cathode reaction (reaction 2) give rise to a gas-lift effect, which enhances mass transport of reactants to the electrode surfaces. Chlorine formed on the anode (reaction 3) is dissolved in the electrolyte and reacts to form chlorate through a number of reaction steps (reactions 4-6), see [1].

Overall reaction:

$$NaCl(s) + 3H_2O(l) \rightarrow NaClO_3(s) + 3H_2(g) \quad (1)$$

Cathode reaction:

$$2H_2O + 4e^- \rightarrow H_2 + 2OH^- \quad (2)$$

Anode reaction:

$$2Cl^- \rightarrow Cl_2 + 2e^- \quad (3)$$

Chlorate is formed in a series of chemical reactions:

$$Cl_2 + H_2O \rightarrow ClOH + Cl^- + H^+ \quad (4)$$

$$ClOH \leftrightarrow ClO^- + H^+ \quad (5)$$

$$2ClOH + ClO^- \rightarrow ClO_3^- + 2H^+ + 2Cl^- \quad (6)$$

The chlorate-forming reaction (reaction 6) proceeds slowly, having its highest rate at pH 5.8 to about 6.5, and is strongly dependent on temperature [1]. To achieve the highest possible reaction rate and a low amount of chlorine in the outlet gases the pH in the bulk is therefore in the industrial process commonly around 6-7.

1.1.1 Oxygen evolving side reactions

The current efficiency in the chlorate process is commonly 93-95 % [3]. The deviation from 100 % is caused by the occurrence of side reactions in the bulk and on the electrodes as well as Cl_2 escaping with the cell gas. The major by-product is oxygen, which is evolved either electrochemically on the anode or through homogeneous decomposition of hypochlorite (ClO^-) and hypochlorous acid (ClOH). Oxygen in the cell gas not only affects the energy consumption, but is also considered as a safety risk. Too much oxygen could cause an explosion if reacting with the hydrogen evolved at the chlorate cathode.

Some suggested anode reactions giving oxygen are [4,5]:

$$12ClO^- + 6H_2O \rightarrow 4ClO_3^- + 12H^+ + 8Cl^- + 3O_2 + 12e^- \quad (7)$$

$$ClOH + H_2O \rightarrow 3H^+ + Cl^- + O_2 + 2e^- \quad (8)$$

$$2H_2O \rightarrow O_2 + 4H^+ + 4e^- \quad (9)$$

Instead of hypochlorite forming chlorate through reaction 6, as desired, it may decompose to oxygen and chloride in the bulk [4,5].

$$2ClO^- \rightarrow O_2 + 2Cl^- \quad (10)$$

Kotowski *et al.* and Hardee *et al.* [4,5] claimed that reactions 7, 8 and 10 are responsible for the major part of the oxygen evolved in a chlorate cell. However, Tilak *et al.* [6] argued that the primary source of oxygen is anodic discharge from water molecules, and that hypochlorite may contribute to additional oxygen. However, they also pointed out the difficulties in separating different contributions generating oxygen.

Oxygen evolution through water oxidation is a well studied reaction, however most work is reported for either strongly acidic or strongly alkaline electrolytes [7,8]. The electrode reaction differs between the two cases, the reactant being water (reaction 9) or hydroxide (reaction 11, below), respectively.

$$4OH^- \rightarrow O_2 + 2H_2O + 4e^- \quad (11)$$

In neutral electrolytes, such as chlorate electrolyte, both reactions 9 and 11 may take place. Sato and Okamoto [9] studied the oxygen evolving reaction (OER) on nickel electrodes in sulphate solutions of varying pH and found limiting current densities that depended on OH^- concentration. They concluded that the OER with OH^- as reactant was kinetically favoured at sufficient OH^- concentrations, but with acid electrolyte or higher current densities oxygen evolution proceeds by oxidation of water (reaction 9). When a buffer is added to the electrolyte

its acid-base reaction may serve as a source of OH^- to the electrode reaction (reaction 11). Since chromate buffers at neutral pH it would be interesting to investigate how its presence affects the oxygen evolving reactions, reactions 9 and 11. The chromate buffering reactions are presented in section 1.2.1.

1.1.2 Cathodic side reactions involving hypochlorite and chlorate

Since the chlorate cell is undivided, products formed on the anode may easily reach the cathode, where they may be reduced back to chloride ions in chromate-free electrolyte. To raise the cathodic current efficiency, chromate is added to the chlorate electrolyte, which results in a current efficiency for hydrogen evolution of almost 100 %; the efficiency would otherwise have been considerably lower due to parasitic reactions such as reduction of hypochlorite and chlorate (reactions 12 and 13).

Side reactions on the cathode

$$ClO^- + H_2O + 2e^- \rightarrow Cl^- + 2OH^- \quad (12)$$

$$ClO_3^- + 3H_2O + 6e^- \rightarrow Cl^- + 6OH^- \quad (13)$$

In the absence of chromate the reduction of hypochlorite on iron (the major component in the most common steel electrodes) is mass-transport limited at higher current densities [10]. Reduction of chlorate is highly dependent on cathode material and takes place on iron whereas cathodes of Co, Ni, Mo, Ti, Hg and C do not show any activity for chlorate reduction [11,12].

When adding chromate a thin film of chromium hydroxide, $Cr(OH)_3 \cdot xH_2O$, forms on the electrode surface as it is cathodically polarised [13-15]. The film hinders the parasitic reactions 12 and 13, while still allowing the hydrogen evolution to proceed. The addition is necessary for keeping a high cathodic current efficiency, but has the negative effect of increased overpotential on the anode as well as on the cathode [10,16-18]. Eberil *et al.* [18] as well as Cornell *et al.* [17] discuss the chromate effect on the anode in terms of an adsorption onto the active sites for chloride oxidation. At the chlorate cathode, the effect of chromate on hydrogen evolution is difficult to establish, since in chromate-free chlorate electrolyte the reduction of hypochlorite and chlorate takes place in parallel with hydrogen evolution. Therefore, Cornell *et al.* made experiments in sodium hydroxide solution and showed that a $Na_2Cr_2O_7$ concentration of 2 g/L increases the overpotential for hydrogen evolution by about 20 mV [10].

1.2 Electrolyte parameters

To obtain as high and energy-efficient production rate as possible the process parameters such as electrolyte temperature, pH and chloride and chlorate concentrations all have to be optimised.

1.2.1 pH

The pH in the chlorate cell is approximately 6-7, in order to achieve the highest possible reaction rate for the chlorate-forming reaction (reaction 6) [6]. The addition of chromate enhances the ability to keep the bulk pH neutral due to its buffering effect at a pH of around 6 [1]. The equilibrium between hypochlorous acid and hypochlorite (reaction 5) also buffers at neutral pH [1].

Chromate is involved in a number of equilibria, depending on pH, for instance [19] :

$$2HCrO_4^- \leftrightarrow Cr_2O_7^{2-} + H_2O \quad (14)$$

$$CrO_4^{2-} + H_2O \leftrightarrow HCrO_4^- + OH^- \quad (15)$$

$$CrO_4^{2-} + H^+ \leftrightarrow HCrO_4^- \quad (16)$$

$$HCrO_4^- + H^+ \leftrightarrow H_2CrO_4 \quad (17)$$

For the buffering in chlorate electrolyte, reactions 15 and 16 are the most important reactions. Reaction 16 has its strongest buffering effect at a pH close to its pK_a value, which is reported to be in the range of 5.8-6.5 in water [19-21] . Reaction 15 buffers in the same pH range, and may at equilibrium be expressed as the sum of reaction 16 and the dissociation of water ($H_2O \leftrightarrow H^+ + OH^-$). Below pH 1, the existence of H_2CrO_4 should be considered [19].

Although the chlorate electrolyte is pH neutral, the pH of the electrolyte at the electrode surfaces is far from neutral. The electrolyte at the anode surface is acidic due to production of protons in the hydrolysis of chlorine (reactions 4-6) as well as occurrence of the acidifying side reaction oxygen evolution. The cathode has an alkaline diffusion layer since hydrogen evolution increases pH. Surface pH is highly dependent on current density, with a high current density increasing the pH gradients at the electrodes. Figure 2 shows a schematic picture of how the pH varies between anode and cathode. Byrne *et al.* [22] modelled a chromate-free chlorate cell by taking into account the electrode reactions as well as the hydrolysis of chlorine, and predicted the anode pH to be about 4. The diffusion layer for H^+ at the anode varied along the height of the cell, being infinitely thin at the bottom of the cell and steadily increased with the height to become ~150 μm after 0.2 m.

The acidic anode surface suppresses the side reaction oxygen evolution, favouring chloride oxidation. A decrease in the bulk pH of the chlorate electrolyte would suppress the oxygen evolution even more, but would decrease the rate of chlorate formation (reaction 6) as well. Furthermore, the chlorine gas evolved in the electrode reaction would not dissolve in the electrolyte if the pH were too low, but would escape with the cell gas. The main reaction on the anode, chloride oxidation (reaction 3) is in near-neutral electrolyte not directly dependent on pH,

but competes with the pH-dependent oxygen evolution. However, at low pH (pH < 2) chloride oxidation on RuO_2 becomes affected by the pH [23,24], explained by Fernandez *et al.* [23] as the protons inhibiting the sites active for chlorine evolution.

It would be desirable to predict pH as it has an impact on almost all homogeneous reactions in the chlorate electrolyte and thereby influences the electrolyte composition. Additionally, the pH is important for by-product formation as well as undesired precipitation on the electrodes.

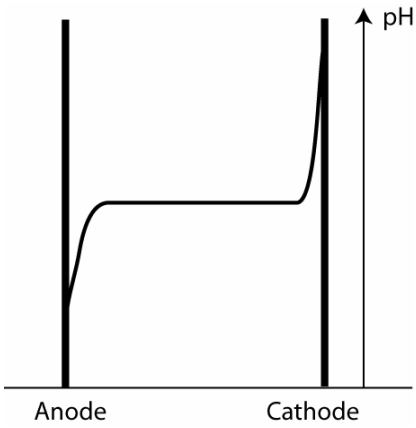

Figure 2. Schematic picture of the pH profile between the two electrodes in a chlorate cell. The pH in the electrolyte bulk is around 6-7 [6].

1.2.2 Temperature

The temperature of the chlorate process is typically 70-80 °C. An increase or a decrease in temperature would lead to a lower current efficiency because the rate of the side reaction oxygen evolution would increase [6]. Increasing temperature results in a higher reaction rate of the chlorate-forming reaction (reaction 6), but also increases the reaction rate of the oxygen-forming side reactions (section 1.1.1). A decrease in temperature would decrease the rate of chlorate formation (reaction 6) and the concentrations of HOCl and ClO^- would build up in the electrolyte, and form oxygen (see section 1.1.1).

1.2.3 Chloride and chlorate concentrations

To avoid mass-transport limitations of chloride and to achieve a low reversible potential for chloride oxidation, saturated chloride brine would be ideal. However, such a high chloride concentration would complicate the crystallisation of the chlorate salt, which is a later step in the production process. Therefore most of the chlorate plants have a sodium chloride concentration of 80-120 g/L [6]. The chlorate concentration is typically around 500-650 g/L.

1.3 The cathode

Since the introduction of the dimensionally stable anode (DSA) in the 1970's the anode overpotential is low, whereas the overpotential of the steel cathode is still very high. The traditional steel cathodes, however have the advantage of being fairly inexpensive but then corrode during stops. In operation the steel is cathodically polarised and thereby protected, but as

soon as the current is switched off it starts to corrode. The chlorate electrolyte is highly corrosive, since it contains the oxidising agents chlorate and hypochlorite. Although the corrosion is disadvantageous in terms of consumption of the steel which reduces the lifetime of the cathodes, it may also be seen as a reactivation process removing deposited impurities and increasing the surface area.

The effect of the electrolyte composition on the chlorate cathode potential is not well investigated. In the literature most studies regarding chlorate-electrolyte conditions concentrate on investigating the current efficiency, see e.g. Ref. [5,6,11,25-29], and a few focus on the DSA-anode potential [16,17,30,31]. For the steel and iron cathodes, polarisation curves at chlorate-like conditions are scarcely presented [10,32,33]. Dobrov and Elina measured polarisation curves on steel in chlorate electrolyte at varied chromate concentration [33]; besides their work no studies on the effect of different electrolyte parameters on the cathode potential have been found. Some of the electrolyte parameters affect hydrogen evolution in general, irrespective of the electrode material, and may be important to consider in the development of new cathode concepts.

With the ambition to decrease the overpotential for hydrogen evolution, extensive work has been carried out on developing activated cathodes for the chlorate process, most of them based on noble metals and titanium. Even though their catalytic activity towards hydrogen evolution has been satisfying they have not been successful - probably not robust enough to survive in the industrial chlorate cell. Lately, higher costs for electricity have triggered intensified activity on the chlorate cathode potential, as shown by several recent patent applications. The approach has been to use electrocatalytic cathode coatings, containing ruthenium [34,35] or electrodeposited Fe-Mo alloys [36,37], as well as divided chlorate cells with coated cathodes [38] or gas diffusion electrodes [38,39]. In the latter case hydrogen evolution has been replaced by the reduction of oxygen as cathode reaction, thereby cutting the cell potential substantially.

1.3.1 The effect of Y^{3+} addition on the cathode reaction

One approach for decreasing the steel-cathode potential could be to in-situ precipitate a catalytically active film on the electrode surface. Ideally, such a film should also hinder parasitic reactions in order for it to replace the chromium hydroxide film of the chlorate cathode used today. As Cr(VI) is ecologically harmful, carcinogenic and reprotoxic it should in the future be replaced by a more environmentally friendly alternative.

Rare earth metals (REM) as replacement for Cr(VI) in corrosion inhibition has been a topic for research during the last 20 years. When REMs are used to prevent corrosion it is possible to take advantage of the spontaneous reduction of oxygen, which normally induces corrosion, but also causes the pH increase necessary for forming REM hydroxides. Dissolved REM salts precipitate as a film of REM hydroxides due to the alkaline surface pH caused by the oxygen reduction. The REM hydroxide films hinder further reduction of oxygen and thereby lower the corrosion rate of the underlying metal [40-46]. Inhibition of oxygen reduction is a characteristic of the chromate film used today and it is reasonable to suspect that the REM films also hinder other cathode reactions, such as hypochlorite reduction.

There are studies showing that an addition of the REM salt, yttrium nitrate, not only hinders the reduction of oxygen by forming an $Y(OH)_3$ film, but also seems to activate the hydrogen evolving reaction [40,41,47]. The activating effect of yttrium on hydrogen evolution was seen by Tran *et al.* [40,41], who made their experiments with iron and gold electrodes, as well as by Hsu and Yen [47] who carried out their measurements on a nickel-base alloy. However, all their studies were made in nitrate-containing electrolytes, which may complicate the interpretation of the results, since nitrate reduction may be difficult to distinguish from hydrogen evolution.

1.4 The anode and the critical potential

During the 1970's the dimensionally stable anode (DSA) replaced the previously used graphite anode. In 1965 Henri Beer had patented his ideas regarding titanium anodes covered with oxides of platinum metals or a mix of platinum metals and oxides of non-precious metals [48]. It was found that ruthenium oxide plus titanium oxide had an extraordinary catalytic activity for chloride oxidation, and not long after Beer's patent the DSAs of TiO_2/RuO_2 were introduced into the chlor-alkali and the chlorate industries. As the name implies the DSA is not consumed during operation as were the graphite anodes, which only had a lifetime of 1-2 years, depending on process conditions. In the chlorate process, the anode overpotential of the DSA is low but the life-time of the ruthenium-based DSA may still be improved. With time or when operated at extreme conditions, the ruthenium-based DSAs used in chlorate electrolysis gradually lose their ruthenium, probably due to corrosion to $RuO_4(g)$, which may escape with the cell gas [49]. The loss of ruthenium leads to higher overpotentials, enhancing the corrosion further and eventually the anodes have to be replaced. Although RuO_4 according to thermodynamics, forms at about 1.4 V vs a normal hydrogen reference electrode (NHE) in chloride-containing solution [49], it is possible to operate RuO_2/TiO_2 DSAs above this potential without immediate loss of ruthenium [50]. Kötz *et al.* [50] suggest that the Ru(VIII) indeed is formed, but may instead of leaving the electrode surface become reduced again as oxygen is evolved. They imply that the two processes probably proceed simultaneously, but that the crystal structure of thermally prepared RuO_2 (as in ruthenium-based DSA electrodes) has stabilising properties, which slow down the corrosion that in fact is much faster at metallic Ru electrodes.

It has been shown [16,17,30] that anodic polarisation curves on dimensionally stable anodes (DSAs) made of RuO_2/TiO_2 bend to a higher Tafel slope at approximately 1.2 V vs Ag/AgCl. The change in Tafel slope is, according to Cornell *et al.* [17], neither related to mass-transport limitations nor to an ohmic drop and would therefore indicate a change in electrode kinetics. The potential and the current density where the polarisation curve bends have been referred to as the critical potential (E_{cr}) and the critical current density, respectively [16]. Eberil *et al.* [16] suggested that the bend at E_{cr} was related to RuO_4 formation. Operating the chlorate process at the current densities for which the polarisation curve has the higher Tafel slope, would obviously give higher potential losses and would as well decrease the current efficiency for chloride oxidation by increased oxygen evolution [25]. In fact, the current efficiency has its maximum at E_{cr} and decreases as the side reaction oxygen evolution increases at potentials below E_{cr} [25]. Operation above E_{cr} could increase the rate of aging of the anode (i.e., the anode loses its ruthenium faster).

The current densities used in industrial chlorate production are usually around 3 kA/m^2, which would result in an anode potential close to E_{cr} [17,30].

It is important to understand how the chlorate process has to be run to avoid exceeding the critical anode potential (E_{cr}) in order to keep the anodic potential losses low and to achieve a long lifetime of the DSA. It would therefore be necessary to evaluate the impact of different electrolyte parameters on E_{cr}. Cornell *et al.* [30] have previously investigated how E_{cr} was affected by changes in chloride concentration at pH 6.5 (typical pH of industrial chlorate electrolyte) and found that E_{cr} decreased with increased Cl^- concentration. However, these results have to be further investigated since at pH 6.5 there is a risk of confusing the impact of Cl^- with the impact of pH on E_{cr}. At bulk pH 6.5, pH at the anode surface differs considerably from the pH in the bulk. Changing the chloride concentration changed the current efficiency for chloride oxidation by the evolution of oxygen, and thereby surface pH changed. By performing the experiments at a much lower pH, the pH gradients at the electrode surface would be negligible, and pH would not change considerably along a polarisation curve. For pH lower than 2, the effect of chlorine hydrolysis on pH (reactions 4-6) is negligible and the effect of oxygen evolution is minor.

1.5 Carrying out experiments at chlorate conditions

Research regarding the chlorate process should of course be carried out at conditions as similar as possible to those of the industrial process, but the experiments performed in an industrial cell are often difficult to interpret.

In the process, studies of effects of electrolyte parameters are complicated to carry out since the parameters are often interconnected. The current density also has a strong impact on the electrolyte conditions. For instance an increase in current density results in higher electrolyte temperature due to the heat generated from ohmic losses. Therefore, polarisation curves at constant temperature are very difficult to measure for industrial cells.

When varying electrolyte parameters and changing other process conditions, their effects on the whole process have to be taken into account and a parameter may have both positive and negative impacts. To separate the different effects of the electrolyte parameters, the influence on the anode and cathode reactions as well as on the homogeneous reactions have to be studied individually.

In the lab cell of this work most parameters may be varied independently of the others, since the measurements are performed during shorter times than in industrial cells and the electrolyte may be replaced instantly when a new composition is required. In the actual process, changes in composition take longer and cannot be varied to the same extent as in the lab.

Even when the results of a study are intended to be applied on the chlorate process, the experiments are not always carried out in chlorate electrolyte. This is when the complexity of the process does not allow a straightforward interpretation of the results. One such example is the study of the anodic side reaction, oxygen evolution (Paper I), which was carried out in 5 M

$NaClO_4$. To isolate oxygen evolution from chloride oxidation and reactions involving hypochlorite, the experiment had to be made in chloride-free electrolyte. However, the electrolyte was still of such high ionic strength and high temperature as to be reminiscent of chlorate electrolyte.

2. AIM OF THIS WORK

The chlorate process is very energy intensive and a major part of the production costs are for electrical energy [2]. Due to the high energy consumption and large production volumes even a small efficiency improvement may save large amounts of energy. The purpose of this work is to identify possible improvements in chlorate electrolysis, with the long-term goal of reducing its energy consumption. Below, more specific goals for the different parts of the project are stated.

The widely used steel cathode has a large overpotential for hydrogen evolution, which could either be reduced by optimising the process parameters further or by developing a new activated cathode. The traditional steel cathodes are still the ones in use and steel or iron are therefore the materials considered in this study.

One approach for activating the cathode reaction could be to in-situ precipitate a catalytically active film onto the electrode surface. Studies made in yttrium(III)-containing chloride electrolyte have implied that the $Y(OH)_3$ film formed on a steel cathode may activate hydrogen evolution [40,41]. The yttrium(III) hydroxide film has inhibiting properties towards oxygen reduction, which is a characteristic of the chromate film used today. Since the chromate film not only hinders oxygen reduction but also prevents the parasitic reduction of chlorate and hypochlorite, it is reasonable to suspect that the $Y(OH)_3$ film might have similar properties. It is necessary from an energy-consumption perspective to obtain a high selectivity for hydrogen evolution on the cathode and it certainly would be an advantage if the toxic chromate in the chlorate process could be replaced by an environmentally friendly alternative, such as e.g. yttrium. The activating effect of yttrium on hydrogen evolution on iron and the selectivity of the $Y(OH)_3$ film have been investigated in this work.

Since the electricity prices are constantly increasing and may also vary periodically, the chlorate plants may be forced to adjust their production rate to the price at each moment in order to minimise their costs. Operation at varying current loads requires knowledge about how the electrodes behave in a wide current-density range. In this work it has been investigated how different chlorate-electrolyte parameters impact the cathode potential for hydrogen evolution at various currents by recording polarisation curves on iron and steel cathodes.

Compared to the cathode, the anode overpotential of the ruthenium-based DSA is small during normal operation but its life-time and its current efficiency towards chloride oxidation may still be improved. It has been found that anodic polarisation curves on DSAs of RuO_2/TiO_2 bend to a higher Tafel slope at ~1.2 V vs Ag/AgCl, and the bend has been associated with the formation of RuO_4 [16,17,30]. The potential for the bend has been referred to as the critical potential (E_{cr}) [16], and operating above E_{cr} could increase the rate of ageing of the anode (i.e. the anode loses its Ru faster). RuO_4 is a gaseous oxide that could escape with the cell gas, which gradually would lead to a deactivation of the anode. Furthermore, operation above E_{cr} gives increased levels of oxygen, thus lower current efficiency for chloride oxidation [25] and the higher Tafel slope above E_{cr} results in increasing potential losses. In order to run the chlorate process at a high production

rate (i.e. high current) without reaching/exceeding E_{cr}, this work has investigated how different electrolyte parameters affect the critical potential.

In the chlorate cell there is a complex interplay between homogeneous reactions, electrode reactions and mass transport. For a better understanding of this interplay modelling of the system is helpful. Although a model of the whole chlorate cell would be interesting, it would certainly be difficult to implement and to interpret without reliable input data and a deeper understanding of the various reactions. Therefore, a simplified system has been simulated, in which water dissociation and pH buffering, due to chromate, interact with the pH-dependent electrode reaction, evolution of either oxygen or hydrogen evolution. The information gained may be used to understand the impact of chromate buffer on the anodic side reaction, oxygen evolution, and on the cathode reaction, hydrogen evolution.

3. EXPERIMENTS AND METHODS

In this section the experimental conditions are presented in brief. For more detailed information the reader is referred to the papers.

3.1 Experimental set-up

All polarisation experiments were carried out in the same type of cell, shown in Figure 3. The cell was a jacketed glass cell connected to a water bath for temperature control.

The working electrode was a rotating electrode, either a rotating disk electrode (RDE) or a rotating cylinder electrode (RCE). Using rotating electrodes gives the possibility to control the mass transport to the electrode surface and to avoid disturbing gas bubbles, formed in the electrode reactions, from attaching to the surface.

The three pictures on the right hand side in Figure 3 show the different types of electrodes used in this work: a standard RDE with a Teflon sheath (top), an RDE punched from a DSA plate and placed into a titanium holder (middle) and a standard RCE (bottom). For the titanium holder, the bare metal was masked with silicon tubing and epoxy to hinder electrochemical reactions taking place on the holder and to avoid capacitances disturbing the current interrupt technique. In the pictures the electrodes are facing upwards but they are turned up-side down when screwed onto the rotating shaft.

The RDE was used in most experiments due to its many advantages. One is that the convective flow pattern in the vicinity of the disk may be analytically expressed [51], and thereby the mass transport to the surface estimated. These analytical expressions allowed modelling of the mass transport-dependent electrode reactions at the RDE without having to solve the convective flow equations. Another advantage is that when surface polishing was required the flat surface of the RDE was preferred since the cylindrical electrode could easily be deformed if not polished with care. For some electrode materials only RDEs could be constructed. Such a material is the DSA, which was not available in cylindrical shape but was punched in disk shape from industrial electrode plates and put in a titanium holder (see Figure 3, second picture from above, on the right hand side).

To investigate whether the DSA in the titanium holder would fulfil the criteria for the plane ideal RDE, a comparison between the Levich equation [51] and experimental limiting currents for ferricyanide reduction on the electrode was carried out. It was shown that the electrode could be regarded as ideal for rotation rates up to 3000 rpm, at least for the ferricyanide system.

Even though in most cases the RDE was preferred to the RCE, the use of RCEs was advantageous at low rotation rates, i.e. when mass transport was poor. At rotation rates lower than 1000 rpm, gas bubbles were trapped below the RDE surface, whereas the cylinder electrode (RCE) allowed the bubbles to rise freely.

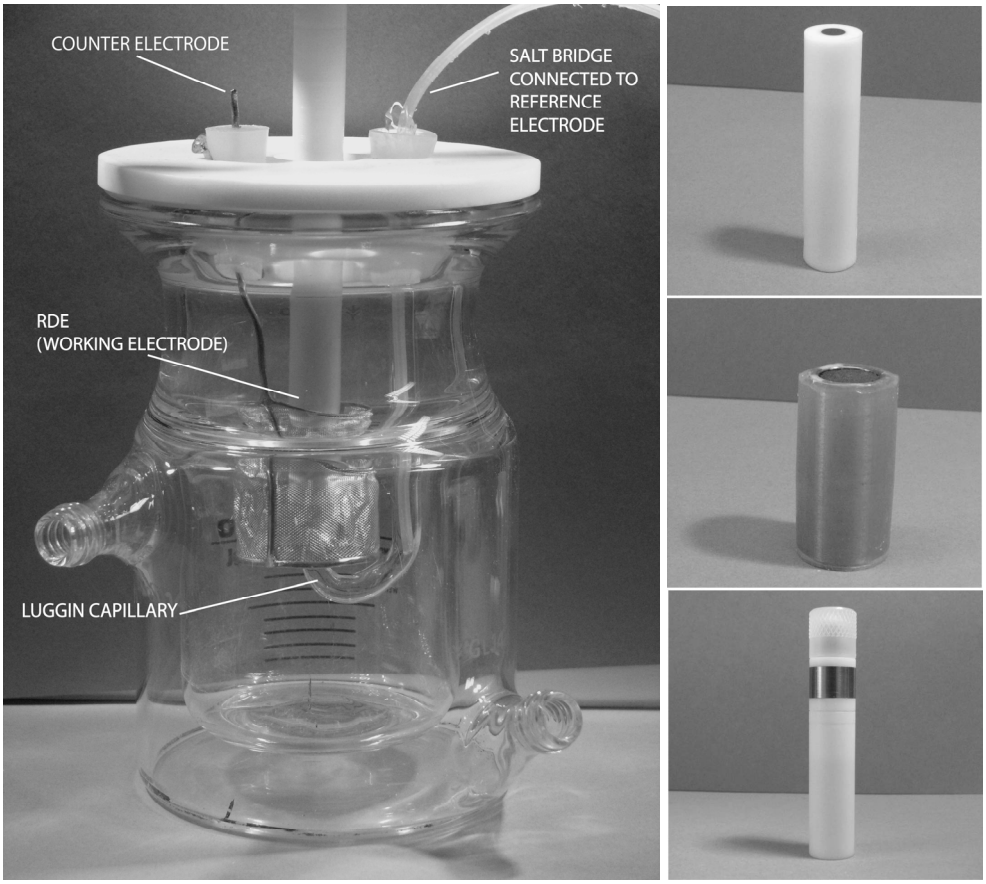

Figure 3. Experimental cell and electrodes. Large picture: Jacketed glass cell with working electrode (in the picture an RDE). Small pictures (top to bottom): Classical RDE, RDE with titanium holder, RCE.

To position the reference electrode (an Ag/AgCl electrode with saturated KCl) a Luggin capillary and a salt bridge, connecting the reference electrode with the cell, was used. The salt bridge contained either NaCl solution or, for chloride-free experiments, $NaClO_3$ solution. In Figure 3 the set-up for the RDE is shown, for which the Luggin capillary points upwards to the centre of the RDE. When using a cylindrical electrode a different Luggin capillary was employed, pointing right through the counter electrode to the side of the cylinder. The counter electrode was a large area platinum mesh electrode.

3.2 Reproducibility and pre-treatment of electrodes

Before recording a polarisation curve the electrode had to be pre-treated to ensure good reproducibility. The treatment depended on the electrode material and differed between cathodes and anodes. Whereas good reproducibility was easily obtained for the DSA anodes, the steel and iron cathodes required greater effort (described below).

3.2.1 DSA anodes

The DSA electrodes were pre-polarised by recording several anodic polarisation curves. This was done until the polarisation curve no longer changed. The pre-polarisation was carried out in electrolyte of the same composition as for the actual measurements. The actual surface area of the electrode may vary slightly between samples and their different pre-histories may cause slight

differences in the appearance of the polarisation curves, even though they were recorded at the same conditions. Therefore, the same sample was used in consecutive measurements when the purpose was to compare polarisation curves at different conditions.

3.2.2 Iron or steel cathodes

To achieve good reproducibility for cathodic polarisation curves on iron and steel it turned out that polishing the surface prior to the experiment and pre-polarising the electrode were very important. Additionally, the electrodes had to be submerged into the electrolyte under cathodic polarisation to avoid corrosion.

Polishing

Good reproducibility was especially important when the effect of changing different electrolyte parameters was studied (Paper III) when even small changes in the potential were of interest. To keep special control of the reproducibility at these experiments, five consecutive polarisation curves were always recorded, with electrolyte pH adjusted and the electrode polished prior to each measurement. Studying the variation between these measurements showed that polishing with emery paper (grade 4000) was to be preferred. However, this could only be done for the RDE, while the RCE required more careful polishing with alumina paste to avoid deformation of the cylindrical shape.

Pre-polarisation

Since iron and steel electrodes would corrode at open circuit they were submerged into the electrolyte under galvanostatic control and thereafter pre-polarised for 2 minutes.

Pre-polarisation of limited time was necessary when recording cathodic polarisation curves. In the case of chlorate electrolyte the time had to be long enough to obtain a chromium film on the electrode, giving a high current efficiency for hydrogen evolution, but short enough not to change the composition of the electrolyte. In all experiments the time of polarisation had to be the same to be able to measure on a similar type of surface, since the surface composition may change with time as surface oxides are reduced and possible impurities precipitate on the electrode surface. On a newly polished electrode the chromate film is formed almost instantly [10] and only a short pre-polarisation of 2 minutes (10 kA m^{-2}) before recording a polarisation curve was considered necessary.

The corroded electrodes needed longer pre-polarisation to reach a high current efficiency [26] and they were therefore operated at 10 kA/m^2, at 3000 rpm, for 1h in a separate chlorate solution. To retain the chromate film, the electrodes were removed from the pre-polarisation electrolyte still under galvanostatic control, and were thereafter rinsed with water to remove electrolyte traces that otherwise could have caused film dissolution. When submerged in the new chlorate electrolyte the electrodes were under galvanostatic control.

3.3 Instrumentation

Galvanostatic polarisation curves were recorded using a PAR273A potentiostat connected to an oscilloscope, Nicolet Integra 20. Correction for iR-drop was made with a current interrupt

technique described by Cornell *et al.* [30], in which potential transients are recorded by the oscilloscope as the current is interrupted.

3.4 Determination of the critical anode potential

E_{cr} and i_{cr} were determined by fitting straight lines to the polarisation curve before and after the bend to the higher Tafel slope. The coordinates for the point where the two lines crossed were defined as (i_{cr}, E_{cr}).

3.5 Modelling

In this section the modelling is described briefly. More details and information about input data is found in the papers (Papers I and III).

The model simulates an RDE cell, in which water dissociation (reaction 18, below) and pH buffering of chromate (reaction 15 or 16) interact with pH-dependent electrode reactions. The electrode reaction is either oxygen evolution or hydrogen evolution. The chromate buffering is in the oxygen-evolving model described by reaction 15 ($CrO_4^{2-} + H_2O \leftrightarrow HCrO_4^- + OH^-$) and in the hydrogen-evolving model by reaction 16 ($CrO_4^{2-} + H^+ \leftrightarrow HCrO_4^-$). The reason for choosing these reactions is further discussed in section 4.1.4.

$$OH^- + H^+ \leftrightarrow H_2O \qquad (18)$$

The model is one-dimensional and the use of the RDE cell allows analytical description of the convective flow [51]. The model is based on mass balances at steady-state for each specie, *i*, in the electrolyte.

$$-\frac{\partial N_i}{\partial z} + R_i = 0 \qquad (19)$$

Where N_i is the molar flux of specie *i* and R_i is the production term. The molar flux, N_i, is expressed by the Nernst-Planck equation, with the migration term neglected.

$$N_i = u_z c_i - D_i \frac{\partial c_i}{\partial z} \qquad (20)$$

where u_z is the convective velocity in the direction perpendicular to the disk surface, D_i is the diffusion coefficient and $\partial c_i/\partial z$ is the concentration gradient of specie *i*. The potential and concentration-dependent electrode reactions are used as boundary conditions; in the bulk electrolyte all concentration gradients are assumed to be zero.

Although chromate is added as $Na_2Cr_2O_7$ to the electrolyte, it is assumed to dissolve into CrO_4^{2-} and $HCrO_4^-$. The species which the model was solved for were H^+ and OH^-, CrO_4^{2-} and $HCrO_4^-$.

Kinetic parameters for the electrode reactions could be extracted from experimentally measured polarisation curves, in a potential region where the electrode reactions were limited by electrode kinetics. These parameters could then be used to model polarisation curves in a wider current-density range where buffer capacity and mass transport sometimes limited the reaction. Simulated polarisation curves were compared with experimental curves at different pH values and chromate concentrations.

The Convection-Diffusion mode of Comsol Multiphysics was used for solving the equation system.

4. RESULTS AND DISCUSSION

This section is a summary of the most important results presented in the appended papers. Before going deeper into the results from experiments made at chlorate conditions, a more theoretical discussion regarding the reactions hydrogen and oxygen evolution is presented. These reactions will reappear throughout the section and it is important to understand their impact on pH profiles in the diffusion layers and how their reaction rates are affected by the presence of a chromate buffer.

Anodic as well as cathodic polarisation curves are presented. In the curves, i_c denotes a cathodic current density, while i_a denotes an anodic current density. When discussing the potential, it is clear that a decreasing potential for the anode means that less energy is needed for the reaction (lower overpotential), while for the cathode a decreasing potential means going to more negative values, i.e. the absolute value of the overpotential is increased and more energy is required.

4.1 The impact of pH buffers on pH-dependent electrode reactions

In the chlorate cell there is a complex interplay between homogeneous reactions, electrode reactions and mass transport. To better understand this interplay modelling of the system is helpful. Although a model of the whole chlorate cell would be interesting, it would certainly be difficult to implement and to interpret without reliable input data and a deeper understanding of the different reactions. Therefore, the model of this section simulates a simplified system, in which water dissociation and pH buffering interact with a pH-dependent electrode reaction. The electrode reaction of the model is either oxygen or hydrogen evolution taking place at the RDE with chromate as pH buffer in the electrolyte. These reactions are of interest since they are both important in the chlorate process. Hydrogen evolution as it is the main reaction on the cathode and oxygen evolution as it is a side reaction to chloride oxidation on the anode. As discussed in section 1.1.1, several oxygen evolving reactions are proposed to take place in a chlorate cell, however, in this model reactions 9 and 11 are considered.

The model was experimentally validated by comparing the modelled polarisation curves with measured ones. Most focus is on the anodic reaction oxygen evolution, and it will be shown that the chromate buffering has a very similar impact on the hydrogen evolved on the cathode. The modelling results would not only be important knowledge in the case of modelling a whole chlorate cell but are also of general interest for understanding of how a buffer interacts with pH-dependent electrode reactions under influence of mass-transport limitations.

The experimental curves for validation of the model were recorded in different electrolytes depending on the electrode reaction studied. For oxygen evolution, 5M $NaClO_4$ electrolyte with and without chromate addition was used, while for hydrogen evolution chromate-containing chlorate electrolyte was employed. The electrolytes were chosen to resemble to chlorate electrolyte, but had to be composed so that the desired electrode reaction could be studied without influence of side reactions. The purpose of using chloride-free $NaClO_4$ electrolyte was to avoid chloride oxidation. However it was of high ionic strength and held at 70 °C to be

reminiscent of chlorate electrolyte. The electrodes were of the same materials as the anode and cathode of the chlorate cell, i.e. a ruthenium-based DSA for chlorate production as anode and an iron cathode for hydrogen evolution.

4.1.1 Experimental polarisation curves for H_2 and O_2 evolution in chromate-free electrolyte

As an introduction to the more complex modelling discussed in 4.1.2, experimental polarisation curves in buffer-free electrolyte for hydrogen and oxygen evolution are presented. It is necessary to first understand how these reactions depend on pH in the absence of added buffer before investigating the impact of a chromate buffer.

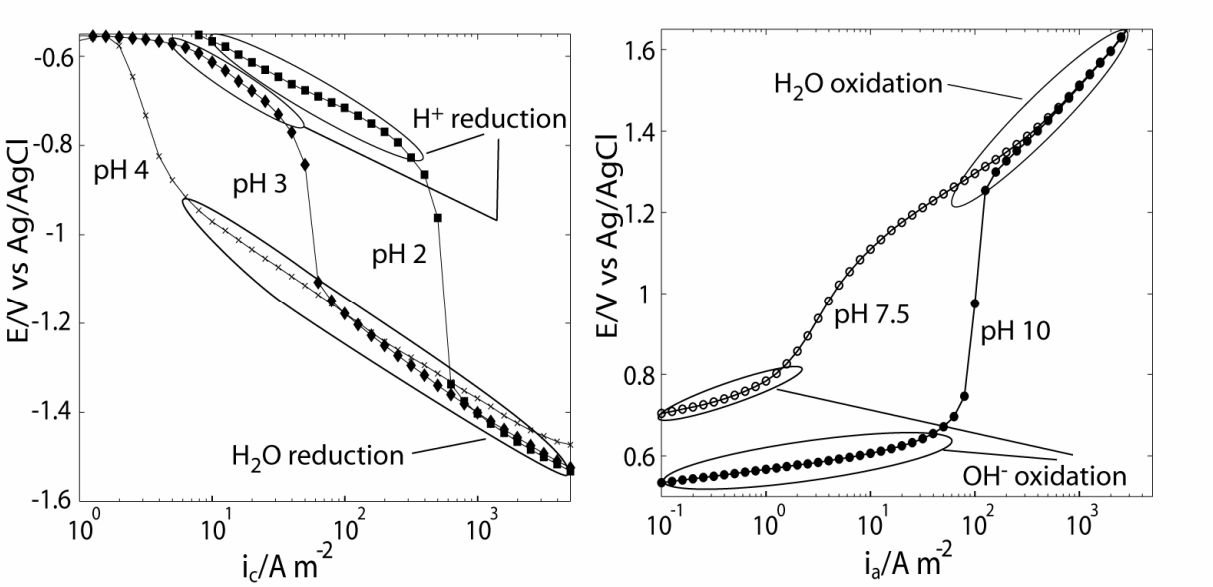

Figure 4. ***(a)*** *Experimental polarisation curves for hydrogen evolution on an iron electrode in chromate- free electrolyte of 0.5M NaCl at 25 °C, 3000 rpm.* ***(b)*** *Experimental polarisation curves for oxygen evolution on a ruthenium-based DSA in chromate-free electrolyte of 5M $NaClO_4$ at 70 °C, 3000 rpm. (In both* ***(a)*** *and (****b****) the regions for the different reactions are shown. The limiting current densities for H^+ reduction and OH^- oxidation, respectively, connect the two regions.)*

In Figure 4a polarisation curves for hydrogen evolution on iron are presented at several electrolyte pH values, and in the absence of chromate. An electrolyte of 0.5 M NaCl at 25 °C was used since the original purpose of the measurements was a comparison with measurements presented later, aiming at investigating the effect of Y^{3+} addition to a 0.5 M NaCl electrolyte. This is a lower ionic strength and a lower temperature than in the chlorate process. However, the main features of the curves are most likely the same even at higher ionic strength and temperature.

Hydrogen evolution on iron proceeds through reduction of H^+ ions (reaction 21, below) or reduction of water molecules (reaction 2) [52]; in Figure 4a these two reactions may be identified. For pH 2 and 3 at lower current densities (~0.6–0.75 V vs Ag/AgCl) the pH-dependent reaction,

H^+ reduction, dominates. This region is interrupted by limiting current densities, due to transport limitations of H^+ to the electrode surface. The current densities are proportional to the H^+ concentration for pH 2 to pH 4, in agreement with the Levich equation [51]. At current densities higher than the limiting current densities, hydrogen is evolved from water (reaction 2). At these high overpotentials, water reduction (reaction 2) is independent of pH since its backward reaction may be ignored.

$$2H^+ + 2e^- \rightarrow H_2 \qquad (21)$$

Polarisation curves for oxygen evolution on a ruthenium-based DSA are presented in Figure 4b. Similar to the polarisation curve for hydrogen evolution, the curve for oxygen evolution is pH dependent at low current densities and pH independent at higher current densities. Whereas oxygen is evolved from OH^- in the pH-dependent region (reaction 11), water is the reactant at higher current densities where the pH has no effect on the potential (reaction 9). The connection between the two regions is a limiting current, due to poor supply of OH^- to reaction 11. Similar polarisation curves have been reported on nickel by Sato and Okamoto [9].

To summarise, at low current densities the pH influences the potential for both oxygen and hydrogen evolution, but at high current densities water molecules are reactants and the reactions are therefore independent of pH. Hydrogen evolution through H^+ reduction is kinetically favoured on the iron cathode at sufficient H^+ concentration, while for anodically evolved oxygen on DSA OH^- oxidation dominates when the OH^- concentration is high enough. When the H^+ and OH^- concentration, respectively, is insufficient both gases evolve by discharge of water (reactions 2 and 9). The limiting current densities for reactions 11 and 21 should be increased in the presence of a buffer that could act as a source of H^+ or OH^-. In chlorate electrolyte chromate would serve as such a buffer through reactions 15 and 16. In sections 4.1.2 and 4.1.3 the effect of chromate on oxygen evolution and hydrogen evolution, respectively, will be discussed.

4.1.2 The effect of chromate buffering on oxygen evolution

Experimental and simulated polarisation curves

In Figure 5a the effect of chromate on oxygen evolution is illustrated by experimentally recorded polarisation curves in 5M $NaClO_4$ electrolyte at pH ~7.5 and pH 10. These two pHs were chosen since polarisation curves recorded at both pHs were affected by addition of chromate (3 g L^{-1} $Na_2Cr_2O_7$, which corresponds to 22.9 mM (CrO_4^{2-} + $HCrO_4^-$)), but the effect appeared differently for each pH. For comparison the polarisation curves in chromate-free electrolyte, already presented in Figure 4b, are also shown. The limiting current densities are clearly affected by addition of chromate, and the largest relative effect is seen for pH ~7.5, where the limiting current density increases by almost two orders of magnitude, up to $2 \cdot 10^2$ Am^{-2}.

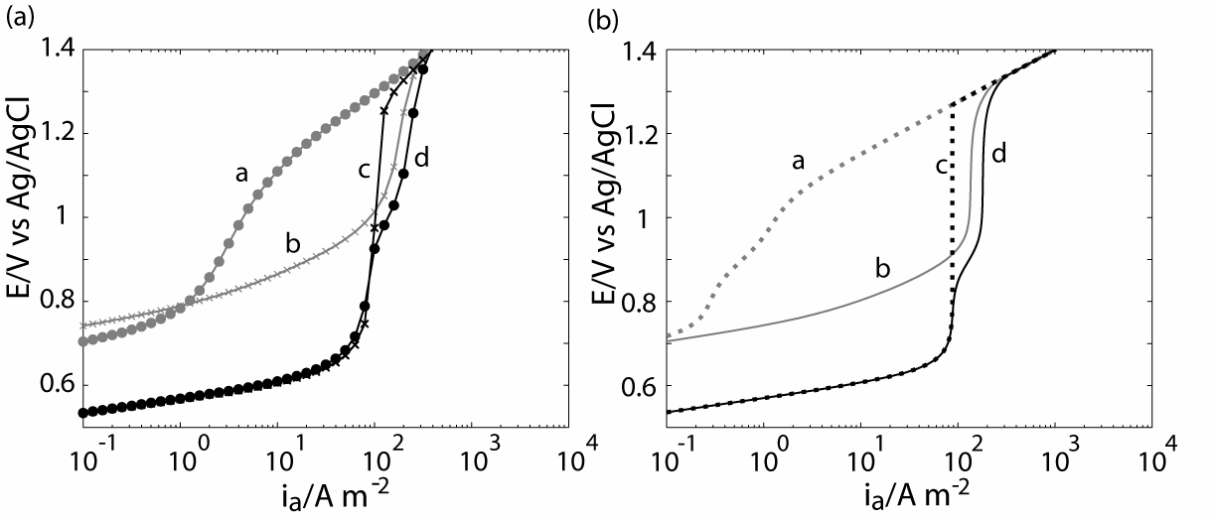

Figure 5. ***(a)*** *Experimental polarisation curves in 5 M $NaClO_4$ electrolyte, at 70 °C and pH 7.5 and pH 10, with and without chromate addition, 3000 rpm, ruthenium-based DSA: (a) pH 7.6, chromate-free, (b) pH 7.3, 3 g/L $Na_2Cr_2O_7$, (c) pH 10, chromate-free and (d) pH 10, 3 g/L $Na_2Cr_2O_7$.* ***(b)*** *Simulated polarisation curves in 5 M $NaClO_4$ at 70 °C and pH 7.5 and pH 10, with and without chromate addition, 3000 rpm: (a) pH 7.5, chromate-free, (b) pH 7.5, 3 g/L $Na_2Cr_2O_7$, (c) pH 10, chromate-free and (d) pH 10, 3 g/L $Na_2Cr_2O_7$.*

With a the input parameters presented in Paper I, Table 1, the model succeeds in capturing the increases in current densities obtained from chromate addition, and the simulated polarisation curves (Figure 5b) agree well with the experimental curves (Figure 5a). It should be noted that reaction 15 ($CrO_4^{2-} + H_2O \leftrightarrow HCrO_4^- + OH^-$) represents the chromate buffering in the model. The curves could be studied in more detail to further compare the simulations with the experiments. For bulk pH 10 (curve d in Figure 5a and b), chromate does not affect the limiting current density at the start of the limiting current plateau, but higher up on the plateau an effect is seen (~0.9 V versus Ag/AgCl). There, an increase in current density is observed and a second plateau is reached. This second limiting current plateau due to chromate buffering is clearly seen in the experiments as well as in the simulation. It arises since the pOH at the electrode surface at this point reaches a value where chromate starts to buffer, and reaction 15 supplies OH^- to the electrode reaction. In the low current density region for oxygen evolution from chromate-containing pH 10 electrolyte, an almost straight Tafel slope may be seen (curve d, Figure 5a and b, 10^{-1}–10^{1} Am^{-2}), whereas for chromate-containing pH 7.5 electrolyte, the shape of the polarisation curve is slightly curved (curve b, Figure 5a and b, 10^{-1}–10^{1} Am^{-2}). These shapes are found in both experiments and simulations. The disagreement between simulations and experiments appears at the limiting current plateau for oxygen evolution from chromate-free electrolyte at pH ~7.5 (curve a, Figure 5a and b, ~0.8–1.1 V). The experiment shows a higher limiting current density than the simulation does. This may be attributed to the difficulties in maintaining a fixed pH in non-buffered solutions. The simulated transition region between OH^- and water as reactants appears in two stages (0.7–0.9 and 0.9–1.1 V, curve a in Figure 5b), and the limiting current density exhibits a double s-shape; not well resolved in the experimental curve.

Simulated concentration profiles

To get a better picture of the role played by mass transport in combination with the chromate buffering and water dissociation reactions it is useful to investigate the simulated concentrations as function of the distance from the electrode surface (Figure 6a–c). The potentials, for which the concentrations are plotted, were chosen so that at least one profile for every part of the polarisation curve would be represented; a potential profile at a current density lower than the limiting current density, at the limiting current density and at a potential where oxygen is evolved from water. Figure 6a presents concentration profiles for OH^- at different electrode potentials during oxygen evolution in a chromate-free electrolyte at pH 10. At 0.55 V, the profile has the expected appearance of oxygen evolution from OH^- under mixed electrode kinetics and diffusion control, while at the limiting current density at 1.1 V, the surface concentration of OH^- approaches zero. At higher potentials where oxygen evolution from water dominates (1.3 V), the concentration reaches zero already at some distance from the surface. The hydroxide ions diffusing from the bulk are then not primarily used in the electrode reaction, but react with protons, formed at the surface by reaction 9, at a distance of approximately $0.2 \cdot 10^{-4}$ m from the anode. This could also be confirmed by plotting the H^+ concentration and the rate of reaction 18 ($OH^- + H^+ \leftrightarrow H_2O$) as a functions of the distance from the electrode surface.

Figure 6b and c presents concentration profiles for OH^- during oxygen evolution in chromate-free as well as in chromate-containing electrolytes, both at pH 7.5. In both figures, the profile at 0.7 V represents a potential corresponding to a current density below the limiting current density. It has the typical appearance of a process under mixed electrode kinetics and diffusion control. For the higher potentials, an inflection point appears and the profiles become s-shaped. At the limiting current density (for chromate-free electrolyte 0.9 V and for chromate-containing electrolyte 1.1 V), the OH^- concentration at the anode surface is close to zero. Along a limiting current plateau, the simulations show that the OH^- profiles do not change noticeably, although the potential increases. However, a magnification of the area close to the electrode (see insets in Figure 6b and c) shows that with increasing potential the OH^- surface concentration decreases due to a steep gradient near the surface. At current densities higher than the limiting current density, when H^+ is produced in the electrode reaction (reaction 9), the thickness of the diffusion layer increases with increasing potential, and the distance for which the OH^- concentration is close to zero grows (profile at 1.4 V).

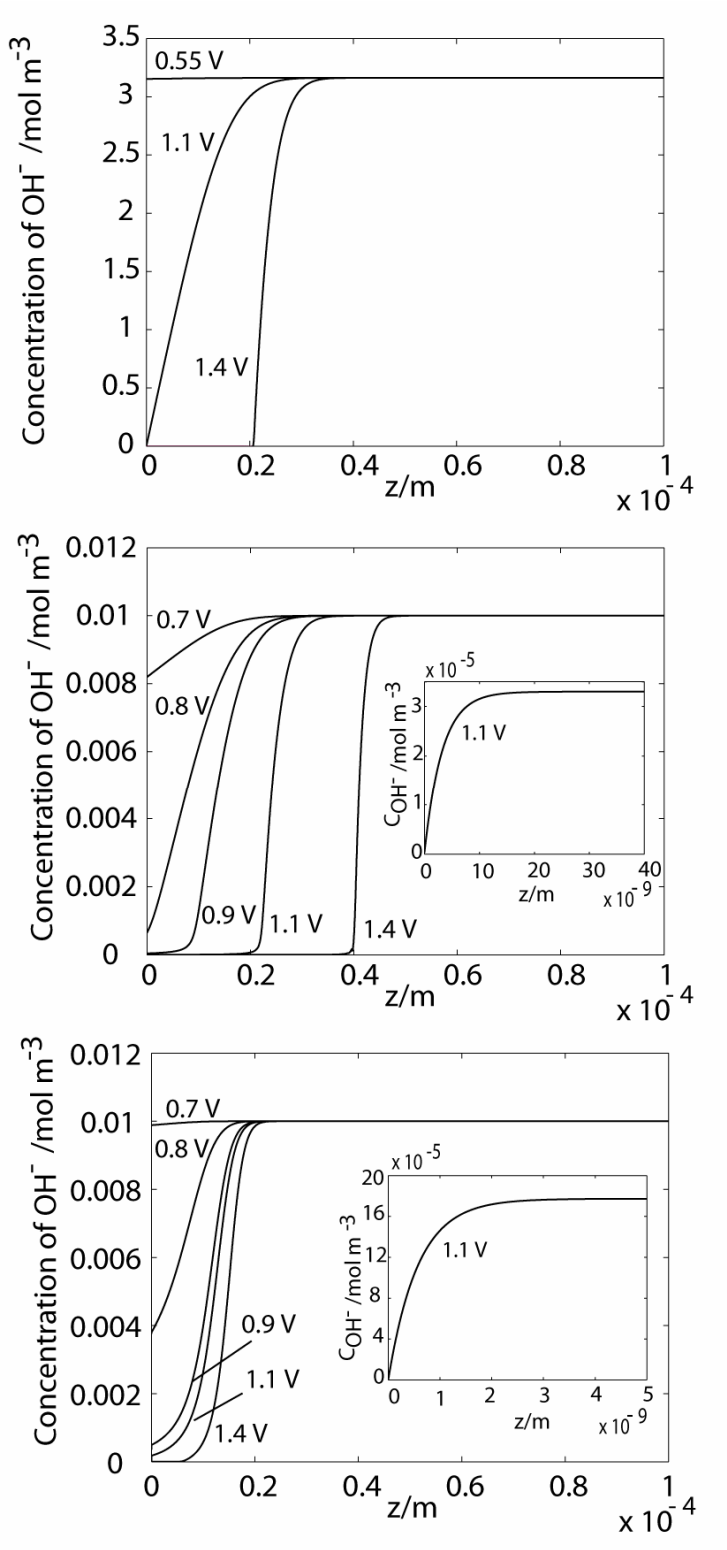

Figure 6. Concentration profiles for OH^- during oxygen evolution in: ***(a)*** *5M $NaClO_4$, 0 g/L $Na_2Cr_2O_7$, bulk pH 10, 70 °C* ***(b)*** *5M $NaClO_4$, 0 g/L $Na_2Cr_2O_7$, bulk pH 7.5, 70 °C and* ***(c)*** *5M $NaClO_4$, 3 g/L $Na_2Cr_2O_7$, bulk pH 7.5, 70 °C. In (b) and (c), the magnification of the profile at 1.1 V close to the anode shows the thin reaction layer. All potentials are vs Ag/AgCl.*

As seen in the insets of Figure 6b and c, the OH^- concentration drops in the very close vicinity of the anode at sufficiently high potentials. This very thin layer (in the orders of nanometers) was defined by Albery [53] as the reaction layer, and when comparing Figure 6b and c its thickness is shown to depend on the presence of chromate. The reaction layer is developed when a homogeneous reaction, such as water dissociation or chromate buffering limits the rate of the electrode reaction. When chromate is present, the buffering reaction (reaction 15) is responsible for the evolution of the reaction layer. As the transport of OH^- from the bulk to the electrode surface becomes limited CrO_4^{2-} ions react through reaction 15 to form OH^- ions, giving rise to an increasing limiting current density. This happens very close to the anode surface, when the CrO_4^{2-} ions are close enough to the anode for the formed OH^- ions to diffuse to the electrode faster than they may recombine with $HCrO_4^-$. The layer where this happens is very thin; for oxygen evolution at pH 7.5 in chromate-containing electrolyte, at 1.1 V versus Ag/AgCl, the thickness is approximately 1 nm. Within the reaction layer, at the same distance from the anode as the OH^- concentration starts to drop, the CrO_4^{2-} concentration levels off, as shown in Figure 7. The CrO_4^{2-} ions may be transported faster from the bulk than the OH^- ions, due to their high bulk concentration (~22 mol m^{-3}) compared to the bulk concentration of OH^- ($10^{-3.6}$ mol m^{-3}).

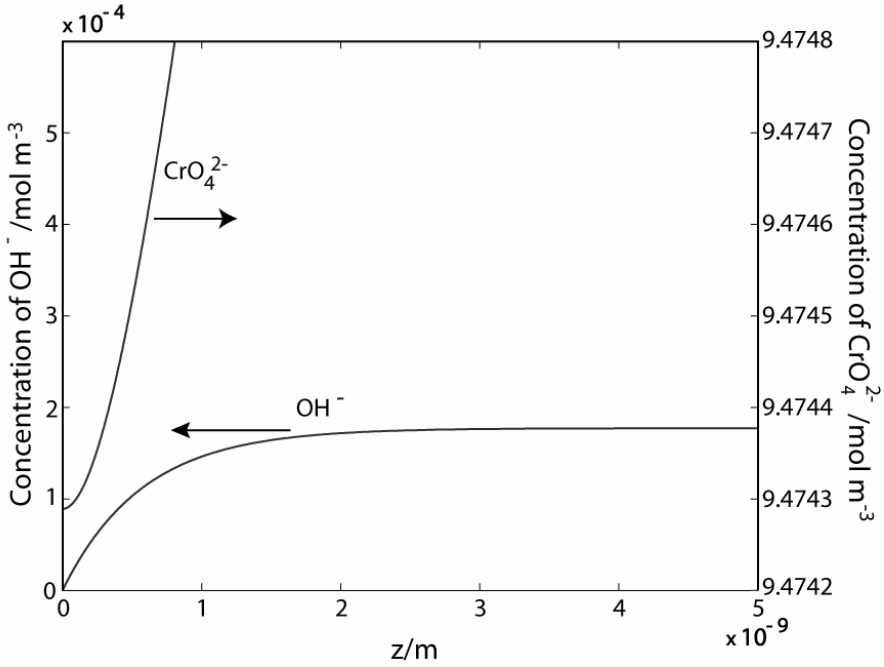

Figure 7. Simulated concentration profiles of CrO_4^{2-} and OH^- in the very thin reaction layer close to the anode (bulk pH 7.5, 5M $NaClO_4$, 3 g/L $Na_2Cr_2O_7$, 70 °C, 3000 rpm, 1.1V vs Ag/AgCl).

The reaction layer is seen to become thinner with a more rapid rate of buffering (reaction 15). With increasing reaction rate the thickness of the reaction layer would approach zero, and the limiting current density would be entirely determined by the mass-transport rate of CrO_4^{2-}.

Interestingly, the simulations show that even when chromate is not present the OH^- profile exhibits a reaction layer (inset of Figure 6b), as water takes the role of a weak base, producing OH^- by its dissociation. However, at the same potential (1.1 V versus Ag/AgCl) this reaction

layer is thicker than with chromate present, at pH 7.5 approximately 10 nm compared to approximately 1 nm. In the case of the chromate-free pH 7.5 electrolyte, the water dissociation give rise to the double s-shape of the transition region between oxygen evolution from OH^- and from water (curve a, Figure 5, ~0.75–1.1 V). The first bend of the polarisation curve (~0.75 V) is attributed to transport limitations of OH^- from the bulk, whereas the second bend (~0.9 V) is associated with the OH^- production due to water dissociation. At higher bulk concentrations of OH^-, such as at pH 10, the transport rate of OH^- is considerably higher than the dissociation of water, thus the water dissociation does not affect the polarisation curve.

The impact of a buffer on oxygen evolution from OH^- may be seen as analogous to the system modelled by Albery [53], in which a weak acid affects the limiting current density for hydrogen evolution from H^+. He assumed the transport to occur only by diffusion, the reaction rate for the weak base to be rate determining for the hydrogen-evolving reaction and the concentration of H^+ to be zero on the anode at limiting current density. He showed that rate constants for the acid/base reaction could be approximated from experimentally determined limiting current densities. From his model the thickness of the reaction layer, at certain conditions, was approximated to 1 nm, which is in the same range as the reaction layers given by the model in this study.

It must be stressed that the electrode is modelled as a planar surface. The thickness of the simulated reaction layer of the model is thinner than the peak-valley distance of the rough surface of the DSA. The appearance of the reaction layer at a rough surface would be interesting to study, but would require more complex models.

The chromate buffer couple ($HCrO_4^-$ and CrO_4^{2-}) may be seen as a shuttle between the outer parts of the diffusion layer and the reaction layer, delivering OH^- to the electrode reaction when transport of OH^- from the bulk is limited. The reaction layer, discussed above, is developed when the OH^- ion produced by reaction 15 ($CrO_4^{2-} + H_2O \leftrightarrow HCrO_4^- + OH^-$) diffuses to the anode surface faster than it recombines with $HCrO_4^-$. This means that in the reaction layer, the chromate buffering reaction (reaction 15) is not in equilibrium. Also the water dissociation (reaction 18) deviates from equilibrium when transport of OH^- from the bulk is limited because of the rapid consumption of OH^- (reaction 11) in combination with the slowness of reaction 18.

Impact of chromate on oxygen evolution in chlorate production

In the chlorate process oxygen evolution is, as earlier mentioned, one of the most important side reactions. The effect of chromate addition is the subject of some controversy. Experimentally, it has been found that the presence of chromate in chlorate electrolyte increased the oxygen content in the cell gas [5,54,55]. Other studies have shown contradicting results [56]. The discrepancy may be explained by the way the studies have been carried out, since there are many factors influencing the oxygen forming reactions. The results may depend on the choice of, for example, anode material, current density, flow pattern, solution composition, pH, and temperature and hence different conclusions may be drawn.

It is therefore desirable to use the results of this study to better understand the factors behind OER as parasitic side reaction, not least the effect of chromate. A typical operating point of a chlorate anode is 3 kAm^{-2} at 1.2 V versus Ag/AgCl [17,30]. The simulations, under conditions of similar bulk pH and chromate concentration as in the chlorate process, show that the current density for oxygen evolution would be approximately 0.1 kA m^{-2}, which corresponds to around 3 % of the total current density. At this point, the current density is limited by the rate of arrival of hydroxide ions formed from chromate in the reaction layer, and thus the OER increases linearly with chromate concentration.

It should be noted, though, that the partial current density of OER in the chlorate cell cannot be assumed to be identical to the one obtained in this study; the mass transport is most certainly different and it is possible that the OER compete for the same active sites as other anode reactions. Additionally, the concentration profiles of chromate, hydroxide and hydrogen ions will be affected by the hydrolysis of chlorine present in the chlorate process. This hydrolysis process has acidifying effects, but it is also buffering at a neutral pH [57]. The buffering of hypochlorite could promote oxygen evolution from OH^-, in an equivalent manner to that of chromate, through reaction 22 (a variant of reaction 5, in alkaline environment).

$$ClO^- + H_2O \leftrightarrow ClOH + OH^- \qquad (22)$$

To make a more accurate prediction of the oxygen-evolving current, chloride oxidation as well as chlorine hydrolysis and reactions with hypochlorite have to be included in the model. However, it seems reasonable that the oxygen-promoting function of chromate, when oxygen is produced from OH^-, should be valid even under those conditions.

4.1.3 The effect of chromate buffering on hydrogen evolution

Experimental and simulated polarisation curves

The effect of chromate buffering on the hydrogen-evolving reaction was studied experimentally as well as by simulating polarisation curves. In contrast to the experiments on anodic oxygen evolution, carried out in 5 M $NaClO_4$, the measurements on hydrogen evolution at the cathode were made in chlorate electrolyte (110 g/L NaCl, 550 g/L $NaClO_3$ at pH 6.5 and 70 °C) of two different chromate concentrations. The model for hydrogen evolution neglects the presence of hypochlorite, since there is no addition of hypochlorite in the experiments and the relatively short times for the measurements do not allow significant build-up of hypochlorite concentration. The homogeneous reactions taken into account are therefore the chromate buffering, $HCrO_4^- \leftrightarrow CrO_4^{2-} + H^+$ (reaction 16), and water dissociation (reaction 18). However, in the industrial chlorate cell the electrolyte has a considerable concentration of hypochlorite, which most certainly influences surface pH by its buffering properties (reaction 5), and modelling such a cell would require inclusion of hypochlorite.

In Figure 8 experimental and simulated polarisation curves are shown for two different chromate concentrations, 3 and 9 g/L $Na_2Cr_2O_7$. For both concentrations a good agreement between

experiments and simulations is seen. The increase in limiting current density for H^+ reduction is explained by the buffer serving as a source of H^+ and thereby decreasing the pH-raising effect of the hydrogen-evolving reaction. This is analogous to the effect of chromate on the limiting current density for oxygen evolution from OH^- discussed above. Hurlen *et al.* [58] have studied how hydrogen evolution on iron in chloride electrolyte is influenced by different additions of acetate buffer. They saw a clear relation between increased acetate content and an increased limiting current density for hydrogen evolution from H^+. This is consistent with the increase due to additions of chromate buffer in this study.

The buffering capacity of the electrolyte species must be considered when operating close to the limiting current, since even a small current change may cause a large potential step, and move the potential into a range where the cathodic protection might be lost.

Similarly to anodic oxygen evolution in chromate-containing electrolyte, the buffering for the hydrogen evolving system takes place in a very thin reaction layer (in the order of nanometers) close to the cathode surface. This reaction layer is indicated by a very steep concentration profile for H^+, arising when H^+ produced from the buffering (reaction 16) diffuses to the cathode surface faster that it recombines with CrO_4^{2-}. In the reaction layer, non-equilibrium prevails for the buffering reaction (reaction 16) as well as for the water dissociation (reaction 18).

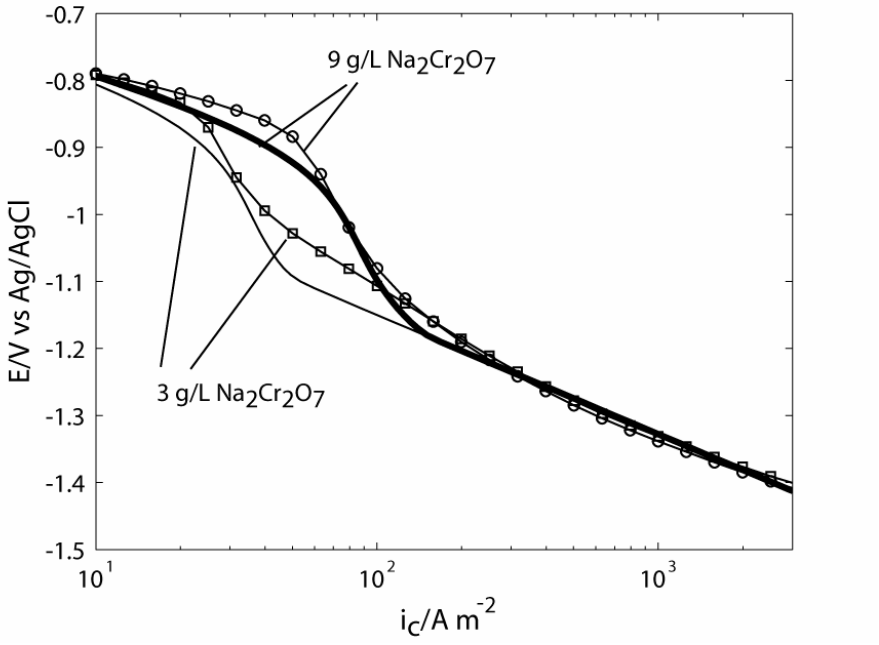

Figure 8. Experimental polarisation curves of hydrogen evolution on an iron electrode in chlorate electrolyte at pH 6.5 (lines with symbols) and simulated polarisation curves (solid lines): 3 g/L $Na_2Cr_2O_7$ and 9 g/L $Na_2Cr_2O_7$, 3000 rpm, 70 °C.

4.1.4 Nature of the chromate reaction

The chromate buffering may be expressed as reaction 15, $CrO_4^{2-}+H_2O \leftrightarrow HCrO_4^{-}+OH^{-}$, or reaction 16, $CrO_4^{2-}+H^{+} \leftrightarrow HCrO_4^{-}$. At equilibrium the buffering may be described in either way, since the sum of reaction 15 and water dissociation (reaction 18), $H^{+}+OH^{-} \leftrightarrow H_2O$ becomes reaction 16. However, as discussed in 4.1.2 and 4.1.3, neither the chromate buffering reactions nor water dissociation are in equilibrium in the reaction layer close to the electrode surface. Thus it became important to differ between reaction 15 and reaction 16.

Depending on the electrode reaction (oxygen or hydrogen evolution), the chromate buffering had to be expressed differently in the model to capture the increase in limiting current densities in the experimental polarisation curves when chromate was added. It was found that the buffering had to directly produce the diffusion-limited ion, since otherwise water dissociation would be rate determining. Whereas reaction 15 had to be used for oxygen evolution, reaction 16 was employed for hydrogen evolution.

Taking the simulation of oxygen evolution as an example, reaction 16 produces no OH^{-}, but may shift the water dissociation reaction (reaction 18, $OH^{-} + H^{+} \leftrightarrow H_2O$) to produce OH^{-} by consumption of H^{+} and thereby increase the limiting current density for oxygen evolution. However, simulations showed that if this reaction (reaction 16) alone were responsible for the buffering, the rate of water dissociation (reaction 18) would have to be increased to unrealistic values in order not to be rate-determining. If the rate of the water dissociation was increased to about 1000 times its literature value (see Paper I, Table 1 [59]), the simulated polarisation curves in chromate-containing electrolyte fitted the experimental curves tolerably. But then for the chromate-free cases, this high water dissociation rate resulted in limiting current densities too high to fit the experimentally measured curves. Therefore, it was concluded that the buffering had to be represented by reaction 15 in the simulations of oxygen evolution. Analogously, the other reaction, reaction 16, had to be used as chromate-buffering reaction in the simulations of hydrogen evolution, since otherwise the rate of water dissociation (reaction 18) had to be increased to an unlikely high rate.

4.2 The critical anode potential

It is important to understand how the chlorate process has to be run to avoid exceeding the critical anode potential (E_{cr}) in order to keep the anodic potential losses low and to achieve a long lifetime of the DSA. The current efficiency may be maximised by operation close to E_{cr} but not above E_{cr}. In the following text, the results from the investigation regarding the impact on the anode potential and on E_{cr} of different electrolyte parameters are presented. Even though changing an electrolyte parameter sometimes does not directly affect the value of E_{cr}, it may, by increasing the anode potential, lead to E_{cr} being reached at lower current densities. As a result, the chlorate process would then be forced to operate at lower production rates to avoid exceeding E_{cr}.

4.2.1 Chloride concentration and pH

Cornell *et al.* have previously found that E_{cr} decreased with increased Cl^- concentration at pH 6.5 [30] (typical pH of industrial chlorate electrolyte). As discussed in the introduction (section 1.4), at pH 6.5 there is a risk of confusing the impact of Cl^- with the impact of pH on E_{cr}. By performing the experiments at a much lower pH, the pH gradients at the electrode surface would be negligible, and the pH would not change considerably along the polarisation curve. Additionally, at strongly acidic pH values, the effect of oxygen evolution is minor and the advantage of a longer Tafel region for chloride oxidation in the polarisation curve facilitates the determination of E_{cr}.

Polarisation curves showing the effect of varying chloride and chlorate concentration at electrolyte pH 2 are presented in Figure 9. The total molar concentration was kept constant at 5 M to fix the ionic strength. As explained above, oxygen evolution is of minor importance in chloride solutions at pH 2, however in the chloride-free case it becomes the electrode reaction. An increase in chloride concentration gave a decreasing potential in the whole potential range, which was explained by a lowered reversible potential and an increased exchange current density for chloride oxidation. The impact of chloride on E_{cr} is illustrated in Figure 10, which shows that E_{cr} decreases with increasing chloride concentration. There was a linear relationship between E_{cr} and the logarithm of chloride concentration with a slope of approximately -90 mV/decade C_{Cl}, which was similar to that found for pH 6.5 [30]. The results of the experiments at pH 2 combined with the results achieved earlier by Cornell *et al.* [30] indicate that there is a direct effect of chloride concentration on E_{cr}.

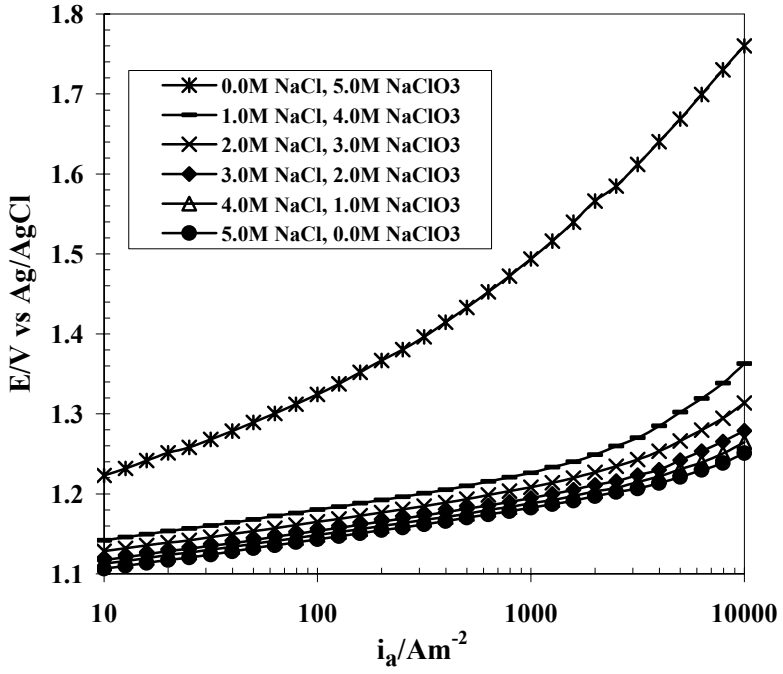

Figure 9. Polarisation curves on DSA in an electrolyte of x M NaCl + (5-x)M $NaClO_3$, 3 g/L $Na_2Cr_2O_7$ at pH 2, and 70±1 °C ($0 \leq x \leq 5$)

With a lowered E_{cr} it might seem that the risk of reaching this potential during operation would increase. This is however not always the case. Even though a higher chloride concentration decreased E_{cr}, the critical current density, i_{cr}, increased with increased chloride concentration. This would mean that the process could be operated at a higher current density when the chloride concentration increases.

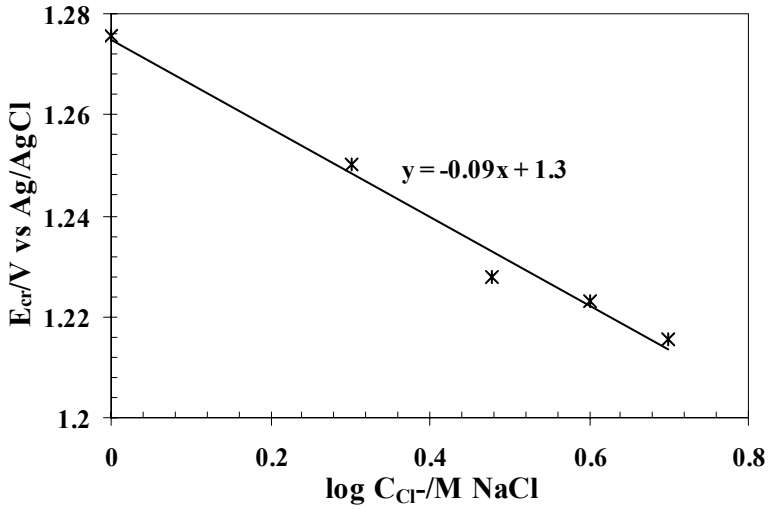

Figure 10. Critical potential, E_{cr}, as a function of the logarithm of chloride concentration. Data from Figure 9.

4.2.2 Temperature and apparent activation enthalpy

The effect of temperature on anodic polarisation curves on a DSA was investigated in a chlorate electrolyte of composition 550 g/l $NaClO_3$, 110 g/l NaCl, 3 g/l $Na_2Cr_2O_7$ at pH 6.5. The polarisation curves had earlier been recorded by Cornell [60] (Figure 11), but had not been further analysed. As expected, the anode potential became higher when the temperature was lowered, due to lower reaction rates, and also E_{cr} became higher. The advantage of the increase in E_{cr} is however outweighed by the increase in anode overpotential when the temperature is lowered. The critical current density, i_{cr}, increased with increasing temperature. As the process is operated at a constant current the risk of exceeding E_{cr} and i_{cr} is actually lowered when operating at a higher temperature, this agrees with results of Eberil *et al.* [16].

The apparent activation enthalpy was derived from the polarisation curves in Figure 11 (for details see Paper II). By plotting $\log(i)$ vs $1/T$ at constant potential, the activation enthalpy, ΔH_a, could be derived from the slope of the curve (Eq. 23).

$$\log i = \log k_a' - \frac{1}{\ln 10}\frac{\Delta H_a}{RT} \qquad (23)$$

The activation enthalpy for an anodic reaction may, as an approximation, be expressed as

$$\Delta H_a = \Delta H_a^0 - \alpha_a FE \qquad (24)$$

Since the ΔH_a values at all potentials were more or less a mixture of the activation energies for oxygen evolution and chloride oxidation, the enthalpy derived through Eq. 23 was called the apparent activation enthalpy. In Figure 12, the apparent activation enthalpy is shown as a function of potential. The diagram shows two linear regions, one at potentials between approximately 1 and 1.1 V vs Ag/AgCl and another between approximately 1.17 and 1.25 V vs Ag/AgCl. The two regions could be related to the regions dominated by oxygen evolution, at lower potentials, and by chlorine evolution at higher potentials. Between those regions both oxygen and chlorine are evolved. Fitting straight lines to the two regions gave a slope of 188 kJ/(mol V) for the lower potentials and a slope of 147 kJ/(mol V) for the higher potentials.

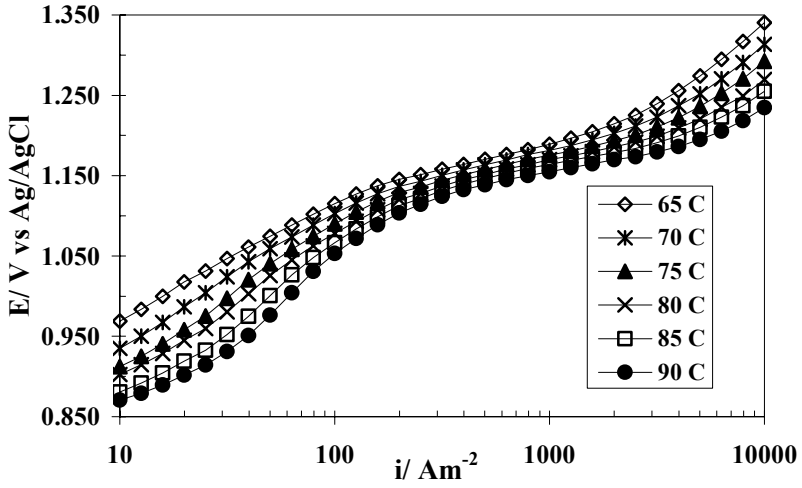

Figure 11. Polarisation curves for different temperatures in chlorate electrolyte (550 g/L $NaClO_3$, 110 g/L NaCl, 3 g/L $Na_2Cr_2O_7$) at pH 6.5 and 65 °C (◇), 70 °C (∗), 75 °C (▲), 80 °C (×), 85 °C (□) and 90 °C (●) [60].

According to Eq. 24, ΔH_a decreases linearly with the potential. Plotting the apparent reaction enthalpy vs. the potential as in Figure 12 would then give a slope of $\alpha_a F$. The linear relation was, as earlier mentioned, only seen in the regions where a single reaction dominated (oxygen evolution or chloride oxidation). The α_a values calculated from the slopes of Figure 12 would according to Eq. 25 correspond to a Tafel slope of approximately 35 mV for lower potentials (oxygen evolution) and a Tafel slope of approximately 45 mV for higher potentials (chloride oxidation), at 70 °C.

$$\text{Tafel slope} = \frac{\ln 10 \cdot RT}{\alpha_a F} \qquad (25)$$

These Tafel slopes were compared to the slopes of the curves in Figure 9 and Figure 11 and to Tafel slopes for oxygen evolution and chloride oxidation found in literature. At lower potentials, mass transport of hydroxide ions influenced the current density for oxygen evolution (reaction 11), which means that the concentration of reacting species at the anode surface at a constant potential was not the same for all temperatures. The Tafel slope calculated from the α_a values extracted from the slope in Figure 12, may therefore disagree with the Tafel slopes for oxygen evolution found in the literature. For oxygen evolution Trasatti [61] found that most studies showed a Tafel slope of 40 mV on RuO_2 electrodes. On RuO_2/TiO_2 anodes Tafel slopes between 35 mV [62] and 66 mV [63] in acid solutions and 30 mV and 50 mV in alkaline solutions [64-66] have been found.

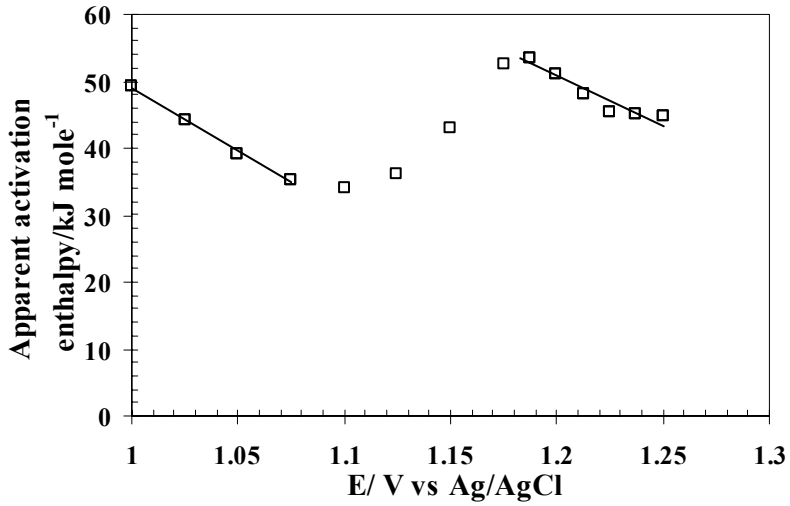

Figure 12. Apparent activation enthalpy for electrolysis in chlorate electrolyte as a function of potential. Straight lines are fitted to the regions where oxygen evolution (lower potentials) and chlorine evolution (higher potentials) are assumed to take place. Chlorate electrolyte concentration 550 g/l $NaClO_3$, 110 g/l NaCl, 3 g/l $Na_2Cr_2O_7$ at pH 6.5.

As mentioned above, the value of α_a for chloride oxidation derived from the enthalpy data in Figure 12 corresponds to a Tafel slope of 45 mV/decade of current. The polarisation curve at 70 °C in Figure 11, showed a slope of approximately 60 mV in the potential range 1.16-1.20 V vs Ag/AgCl. However, this value was not easily estimated for the short linear part of the polarisation curve where chloride oxidation dominates while there is also an influence of oxygen evolution on the slope. The Tafel slope for chloride oxidation at pH 2 (Figure 9) was easier to determine, since oxygen evolution had minor influence at that pH and there was a constant slope ranging over at least two decades of current. The polarisation curves in Figure 9 had Tafel slopes of approximately 40 mV, independent of chloride concentration. This agrees

with most studies on chloride oxidation, which according to Trasatti [67] have found Tafel slopes of 28-40 mV on oxide electrodes.

At potentials higher than E_{cr}, the slope of the polarisation curve in Figure 12 increased even though the value of α_a calculated from Figure 12, was constant. This indicated that the mechanism for the bending of the curve was much less temperature dependent than the chloride oxidation reaction and that the chloride oxidation reaction did not change mechanism at potentials above E_{cr}. The hypothesis, that the mechanism of the chloride oxidation reaction remains the same when increasing the potential above E_{cr}, is supported by the fact that the apparent reaction order with respect to chloride was close to one also at potentials higher than E_{cr}.

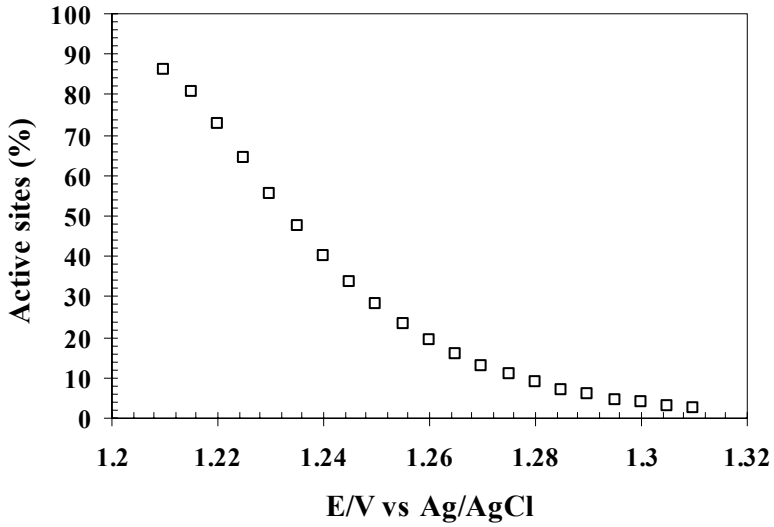

Figure 13. The percentage of active sites left was calculated by dividing the real current density by the current density extrapolated from the Tafel slope. Data for the plot is taken from a polarisation curve recorded in an electrolyte containing 2 M NaCl + 3M $NaClO_3$ at pH 2 (Figure 9).

The higher slopes of the polarisation curves at potentials above E_{cr} could be an effect of a reduction in the number of active sites. If E_{cr}, as earlier mentioned, is assumed to be related to oxidation of ruthenium, then the oxidation could be the reason for the deactivation. The oxidised sites may be less catalytically active for chloride and water oxidation. The reduction in the number of active sites was approximated from the polarisation curves in Figure 9, by extrapolating the constant Tafel slope found for potentials below E_{cr} and assuming the slope to express the current density for which no deactivation of sites had taken place. The percentage of active sites left was calculated by dividing the real current density by the current density extrapolated from the Tafel slope. The result of the calculation, based on the polarisation curve recorded in an electrolyte of concentration 2M NaCl + 3M $NaClO_3$ at pH 2, is shown in Figure 13. The oxidation would, according to Figure 13, be potential dependent, perhaps because some of the active sites would be more sensitive to potential increases while other would require higher potentials to oxidise. If the chloride oxidation would have the same mechanism at potentials

higher than E_{cr}, the current density would increase at the active sites left and thereby increase the potential. Further work would be necessary to verify the hypothesis of deactivation as the reason for the bend to higher Tafel slopes at E_{cr}.

4.3 The impact of different chlorate-electrolyte parameters on hydrogen evolution on iron

The demand for operating the chlorate process at varying current loads requires increased understanding of how the cathode behaves in a wide current-density range under different electrolyte conditions. Therefore cathodic polarisation curves were recorded for iron at various electrolyte compositions. Note that when cathode potentials are discussed a decreased potential means going to more negative values, i.e. increasing the overpotential.

4.3.1 Chromate and hypochlorite concentrations

Figure 14 illustrates the impact of chromate and hypochlorite concentrations on the cathodic polarisation curve for iron in chlorate electrolyte. As discussed in 4.1.3 the most evident effect of an increased chromate concentration is seen at -0.85 to -1.1 V, where the limiting current density, due to poor supply of H^+, appears and the buffering properties of chromate become important. At current densities higher than the limiting current density the consequence of increasing the chromate content from 3 g/L $Na_2Cr_2O_7$ to 9 g/L is only a minor decrease in cathodic potential (less than 20 mV). The chromate film has been shown to increase in thickness with increasing chromate concentration in the electrolyte [68], which may impact the rate of hydrogen evolution.

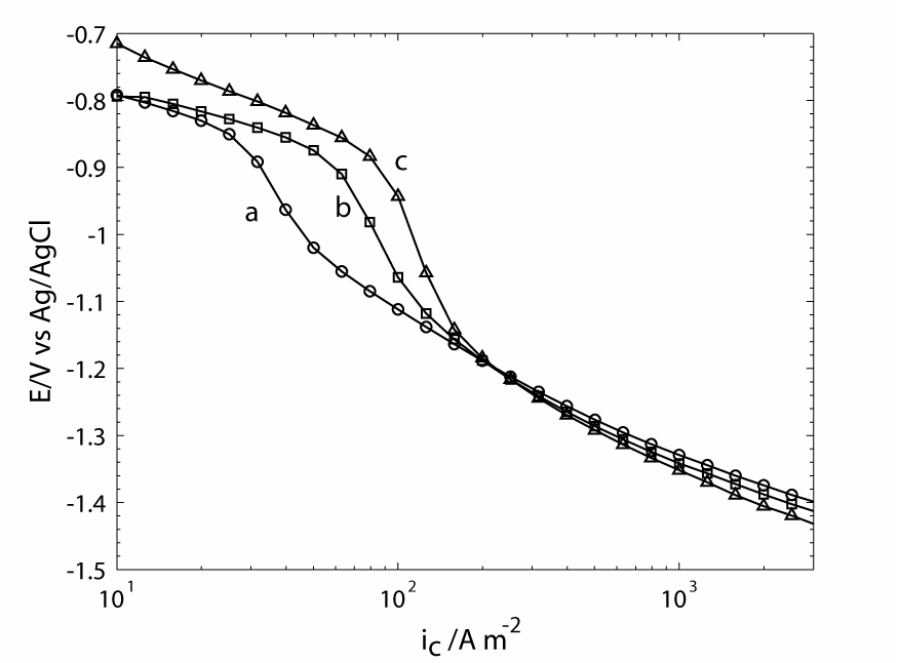

Figure 14. Polarisation curves on a pure iron RDE in chlorate electrolyte (550 g/L $NaClO_3$, 110 g/L NaCl)) at pH 6.5, 70 °C, rotation rate 3000 rpm, with (a) 3 g/L $Na_2Cr_2O_7$, (b) 9 g/L $Na_2Cr_2O_7$, (c) 3 g/L $Na_2Cr_2O_7$ and ~1 g/L NaClO.

Hypochlorite added to the electrolyte particularly affects the limiting current density, by increasing it (Figure 14). At current densities lower than ~10^2 Am^{-2} the presence of hypochlorite increases the cathode potential. This is possibly due to the chromate film not totally hindering hypochlorite reduction. Hypochlorite reduction is limited by mass transport at higher current densities, and the increase in limiting current density seen in Figure 14 may be a mixed limiting current due to limited supply of H^+ and transport-limited hypochlorite. Similar to chromate, hypochlorite acts as a buffer through reaction 5 which would supply H^+ to the hydrogen evolution reaction and increase the limiting current density for reaction 20.

4.3.2 Chloride and chlorate concentrations

On the chlorate anode high concentrations of sodium chlorate (>600 g/L) increase the potential at high current densities (> $3 \cdot 10^3$ Am^{-2}) [17]. To investigate whether a similar effect of increased ionic strength could appear at the cathode, the sodium chlorate concentration was varied between 450 g/L and 650 g/L, keeping the sodium chloride concentration constant at 110 g/L. The polarisation curves from these measurements (displayed in Paper III) show that, similarly to the anode, the increase in chlorate concentration had a negative effect on the cathode potential. In the area where hydrogen evolution from water (reaction 2) is dominating (~$5 \cdot 10^1$ – $3 \cdot 10^3$ Am^{-2}) an increase of the sodium chlorate concentration from 450 to 650 g/L gave around 30 mV decrease in cathodic potential.

To compare the impact of chloride concentration polarisation curves were recorded for 5M (292 g/L) NaCl and 5M (532 g/L) $NaClO_3$ respectively. The chloride solution gave a slightly lower cathode potential for water reduction, by approximately 10-30 mV, compared to the pure chlorate electrolyte.

4.3.3 Temperature

In Figure 15 polarisation curves on an iron cathode in chlorate electrolyte at four different temperatures are displayed. At low current densities where hydrogen is evolved from H^+ reduction (<~$3 \cdot 10^1$ Am^{-2}) the temperature had a minor influence on the potential, but in the current density region (~3kAm^{-2}) where industrial cells on full load are operated and hydrogen is evolved through water reduction, there was a clear increase in cathode potential with higher temperature. This behaviour is expected since a higher temperature increases the reaction rate. Plotting the potential, at constant current density, as function of temperature gives an almost straight line. For a current density of 1 kAm^{-2} the potential increased with 1.9 mV/°C, while for 3 kAm^{-2} the potential increased with 1.6 mV/°C. As mentioned in section 1.2.2 70-80 °C is considered to be the optimum temperature [6] for the chlorate process, since both lower and higher temperatures would increase the oxygen-forming side reactions. Tilak and Chen [6] proposed that a higher temperature would not only increase the rate of the electrode reactions, but also increase the rate of the oxygen-forming side reactions. They propose that a lower temperature would decrease the rate of chlorate formation through reaction 6 and high concentrations of hypochlorite and hypochlorous acid would be built up through reactions 4 and 5. The hypochlorous acid and the hypochlorite would then react to form oxygen. In Paper II it

was shown that the potential for chloride oxidation on the anode (reaction 3) decreases with increased temperature by 1 mV/°C at 1 kAm^{-2} and by 2 mV/°C at 3 kAm^{-2}. Increasing the temperature by 10°C at 3 kAm^{-2} would consequently lower the total cell potential with by at least ~35 mV, which corresponds to approximately 1 % of the cell potential (normally ~3 V), and would of course affect the iR-losses as well.

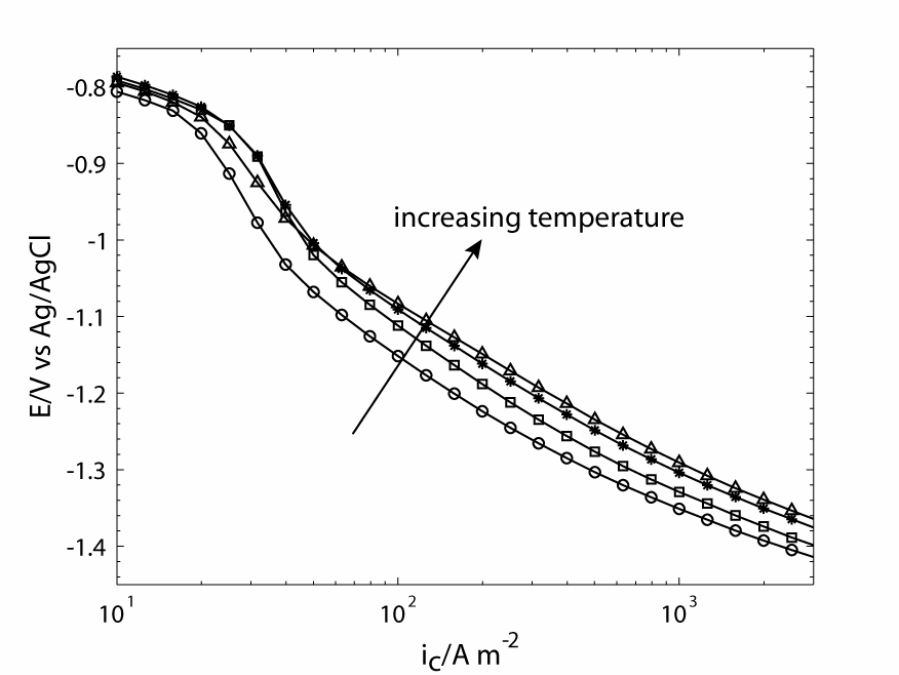

Figure 15. Polarisation curves on a pure iron RDE in chlorate electrolyte (550 g/L $NaClO_3$, 110 g/L NaCl, 3 g/L $Na_2Cr_2O_7$) at pH 6.5, rotation rate 3000 rpm; (○) 61 °C, (□) 70 °C, (■) 83 °C, (◿) 92 °C.

4.4 Hydrogen evolution on corroded steel electrodes

The steel cathodes in industrial cells have electrolyte impurities precipitated on the surface and are usually corroded after having lost their cathodic protection during production stops. These are factors that influence the catalytic activity of the electrode. In Figure 16 polarisation curves in chlorate electrolyte on corroded steel electrodes punched from industrial cathode plates are compared with polarisation curves on non-corroded steel and pure iron. The corroded steel electrodes had been operated (and thus corroded) in a chlorate plant and then washed with water before being used in the measurements of this study.

Whereas the pure iron electrode behaved almost in the same way as the non-corroded steel electrode (which validates the use of pure iron in as model material for the industrial steel electrodes), the activity for hydrogen evolution increases on the corroded steel surface in the whole current-density range. However the largest increase is found at current densities higher than 50 A m^{-2}, where the overpotential decreases by around 100 mV. This may be compared with results of Cornell *et al.* [10], in which an iron electrode, corroded in chlorate electrolyte, obtained a lowered potential for hydrogen evolution compared to the non-corroded iron. Cornell *et al.* compared polarisation curves for iron electrodes corroded at open circuit with non-corroded iron electrodes. The apparent increase in activity for hydrogen evolution of their corroded electrodes

could be due to a catalysing effect of oxides or an increase in surface area, but in the light of later results [26], the apparent activation effect [10] may also be due to reduction of chlorate. The activity for this side reaction is favoured by the presence of oxides on iron electrodes [10,11] and the chromate film has to be built up properly to avoid confusion between increased activity for hydrogen evolution and an increased current due to side reactions. On corroded steel electrodes a high current efficiency for hydrogen evolution was not achieved immediately, but needed around 1 hour of cathodic polarisation in chlorate electrolyte with 3 g/L $Na_2Cr_2O_7$ at 3 kAm^{-2} to reach a constant level of ~95 % [26]. Therefore, the industrially corroded electrodes were given a protecting chromate film at constant current density for 1 hour in chromate-containing chlorate electrolyte.

Two polarisation curves were recorded for the corroded steel electrodes, one at pH 4.5 and another at pH 6.5. For pH 6.5 (industrial pH) a single reaction seems to dominate, since an almost constant Tafel slope is found for the whole current-density range. Increasing the H^+ concentration by lowering the pH to 4.5 results in an increased potential at lower current densities ($< 2 \cdot 10^2$ Am^{-2}), whereas at higher current densities ($>5 \cdot 10^2$ Am^{-2}) the curve coincides with the curve for pH 6.5. This indicates that for pH 6.5 the only reaction is hydrogen evolved from water (reaction 2), while for pH 4.5 the two different reactions for hydrogen evolution (hydrogen formed from H^+ and from water) may be distinguished. It appears as if the corroded surface activates the reduction of water (reaction 2) more than the reduction of H^+ (reaction 20). Alternatively, H^+ reduction might be somewhat suppressed on the corroded surface and the higher activity displayed for water reduction could also be an effect of increased surface area due to corrosion. Further work is needed in order to investigate the contribution of increased surface area and the catalytic effect of the various corrosion products.

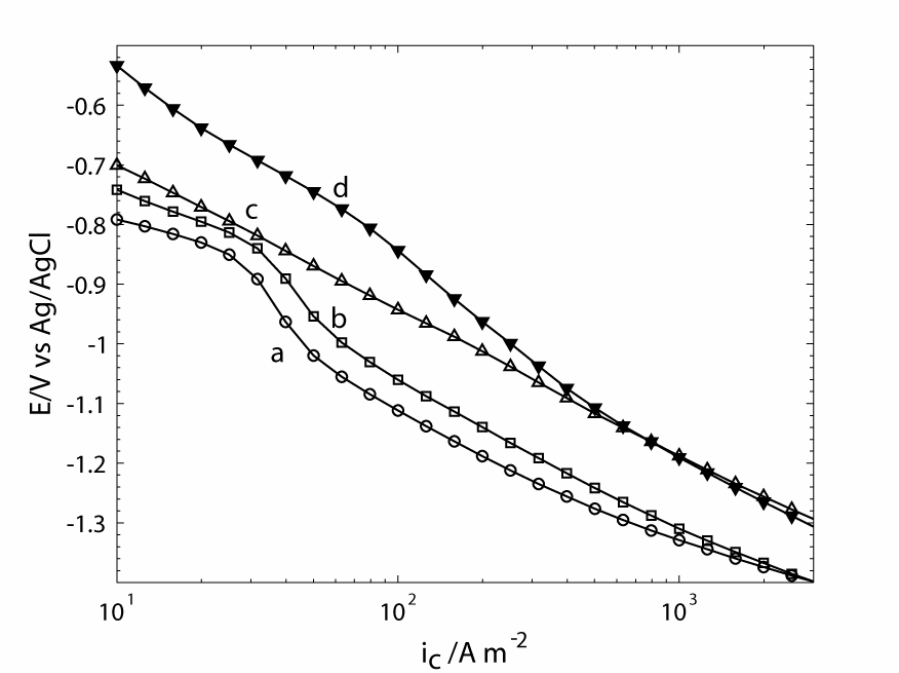

Figure 16. Polarisation curves in chlorate electrolyte (550 g/L $NaClO_3$, 110 g/L NaCl, 3 g/L $Na_2Cr_2O_7$), 70 °C, rotation rate 3000 rpm; (a) pure iron RDE, pH 6.5, (b) polished steel RDE, pH 6.5 , (c) corroded steel RDE, pH 6.5, (d) corroded steel RDE, pH 4.5.

Since no H^+ reduction appeared to take place on corroded steel electrodes, in pH 6.5 electrolyte, the large potential step at the limiting current density for H^+ reduction would not have to be taken into particular consideration when using those electrodes. This may however be important for other cathode materials when electricity prices are high and the process occasionally is operated at lower loads. Then the buffering capacity of the electrolyte species must be taken into account to avoid moving the potential into a range where the cathodic protection may be lost.

4.5 Activation of hydrogen evolution and inhibiting effects in the presence of Y(III)

It is desirable to decrease the high overpotential of the chlorate cathode and replace the toxic Cr(VI) of the electrolyte. One approach would be to in-situ apply a film on the cathode that catalyses the hydrogen evolution while at the same time hindering parasitic reactions from taking place. It is known that a film of $Y(OH)_3$ has hindering properties towards cathodic oxygen reduction [40,41,46] and some studies indicate that the addition of Y(III) to an electrolyte also activates hydrogen evolution [40,41]. It is likely that the $Y(OH)_3$ film hinders other cathodic reactions besides oxygen reduction (e.g. hypochlorite reduction), though no such studies have been found in the open literature.

The $Y(OH)_3$ film may be formed in-situ on the cathode by dissolving Y^{3+} ions in the electrolyte. When cathodic hydrogen evolution takes place, the diffusion layer at the cathode surface becomes alkaline (see reactions 2 and 21) and the dissolved Y^{3+} ions precipitate with OH^- forming a hydroxide film on the alkaline cathode surface according to reaction 26, below.

$$Y^{3+} + 3OH^- \leftrightarrow Y(OH)_3 \qquad (26)$$

Since $Y(OH)_3$ precipitates at a pH of around 7 [69], the electrolyte has to be of lower pH to keep the Y^{3+} ions dissolved.

The effect of addition of yttrium(III) ions on hydrogen evolution on an iron electrode was investigated with focus on a better understanding of the electrochemical properties of the yttrium hydroxide film. In particular its ability to inhibit certain reactions and the possible activation of hydrogen evolution at current densities relevant to industrial electrolysis was of interest. Since this was an introductory study, whose purpose was to understand the properties of the yttrium hydroxide film, the system was simplified by using an electrolyte of lower temperature and lower ionic strength than in chlorate electrolyte, 0.5 M NaCl at 25 °C. At these conditions there was also reference data available to compare the results with [40,41]. The Y^{3+} ions were added to the electrolyte as the salt YCl_3.

4.5.1 Introductory results showing the effects of Y(III)

In Figure 17 the effect of adding 10 mM Y^{3+} to a NaCl electrolyte is illustrated. The polarisation curves were recorded from high to low current densities. With no addition of Y^{3+} the polarisation curve has an almost straight slope at higher current densities (>4 A m^{-2}), where the electrode

reaction is hydrogen evolution. At current densities lower than 4 A m^{-2}, a sharp potential increase appears. This increase is related to the reduction of hypochlorite, generated during the experiment by the counter reaction, chloride oxidation. The steep slope indicates a limiting current density for hypochlorite reduction.

To clearly illustrate the effect of Y^{3+} addition to the NaCl electrolyte Figure 17 has been divided into three regions. Splitting the figure into these regions is only an aid in elucidating the different effects of Y^{3+} visible in this particular figure. With different electrolyte parameters the regions may be shifted or additional effects may be seen. In *Region I*, no major effect of Y^{3+} addition is seen, while in *Region II* the hydrogen-evolving reaction was activated significantly by Y^{3+} addition, i.e. the overpotential decreased by around 200 mV. In *Region III* hypochlorite reduction was hindered by the addition of Y^{3+} and the hydrogen evolution was still activated. The polarisation curve keeps its straight slope from region II into region III, indicating that with Y^{3+} present, the dominating electrode reaction throughout the whole polarisation curve is hydrogen evolution. Yttrium has the same oxidation state, Y(III), throughout the polarisation curve. The only other oxidation state, Y(0) requires much lower potentials (more negative potentials) to form [70]. The catalytic and inhibiting effects of Y(III) addition are further discussed below.

SEM images with EDX shown in Paper IV, Figure 2, indicate that a film of $Y(OH)_3$ is formed at the electrode surface when it is cathodically polarised in Y^{3+}-containing electrolyte at 50 A m^{-2}, i.e. at a current density where activation of hydrogen evolution occurs. The EDX spectra of the SEM image showed that the yttrium-oxygen atomic ratio in the film was 0.3, which corresponds well to the ratio in a dry $Y(OH)_3$ film. Film drying is a problem, since when dry, the film easily detached from the electrode surface and only flakes of yttrium hydroxide could be observed in SEM. Studies of fresh films using an optical microscope indicated a uniform, gel-like hydrous film covering the whole electrode surface. After a few minutes in air, optical microscope photos showed that the film gradually crackled as the water vaporised, which also happened in the SEM at low pressure. This illustrates the difficulty of studying the film ex situ, but in-situ measurements would also be complicated due to gas evolution and requirements on sufficient mass transport. Optical microscope pictures of an electrode operated at the higher current density of 5000 A m^{-2}, where no activation of hydrogen evolution could be seen in Figure 17, showed no film. Nor SEM images and the EDX analysis detected significant amounts of yttrium for an electrode operated at these current densities. This may be due to the vigorous hydrogen evolution not allowing the film to attach or grow thick enough to be detectable.

An yttrium-containing film was also observed in SEM by Tran *et al.* [40,41] who performed experiments on iron and gold in 0.5 M NaCl electrolyte with yttrium added as the nitrate salt, $Y(NO_3)_3$.

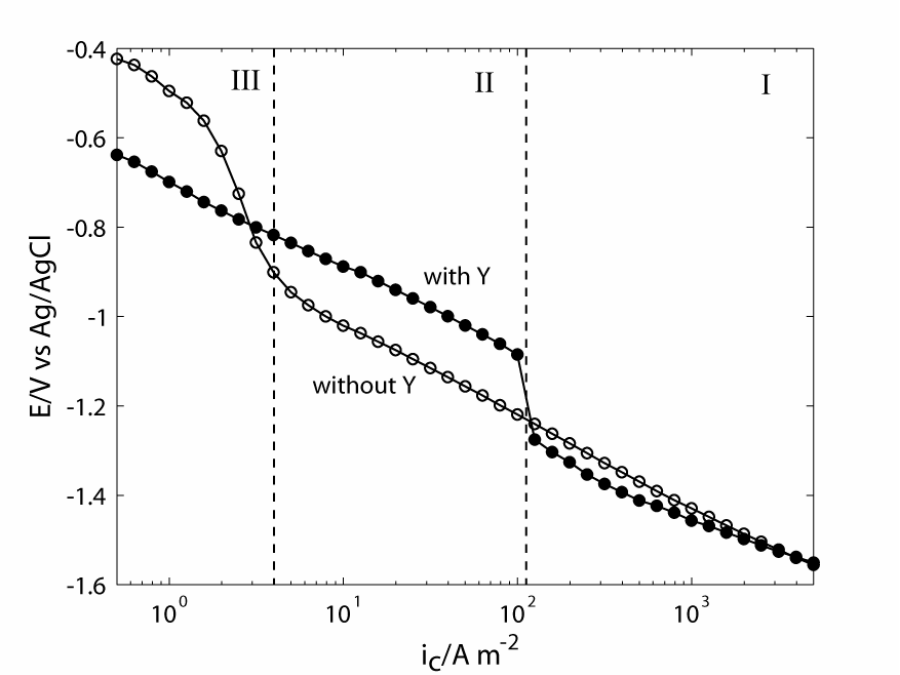

Figure 17. Polarisation curves on iron in 0.5 M NaCl electrolyte with and without Y(III). When Y(III) was added, its concentration was 10 mM and the total Cl⁻ concentration 0.5 M, pH ~6. Yttrium was added as YCl_3. The polarisation curve was recorded from high to low current densities, i.e. in anodic direction.

4.5.2 Activation of hydrogen evolution

The catalytic effect of Y^{3+} in a chloride electrolyte on the overpotential for hydrogen evolution on iron (seen in Figure 17) is also illustrated in Figure 18 where Y^{3+} concentrations of 5 mM and higher may be seen to activate hydrogen evolution. The concentration was varied between 1 and 100 mM Y^{3+} and the results compared with the polarisation curve recorded in yttrium-free electrolyte. A low Y^{3+} concentration, 1 mM, did not activate hydrogen evolution. For a slightly higher concentration, 5 mM Y^{3+}, the activation occurred in two steps as the current density was decreased. Increasing the time of polarisation at each current level from 15 s to 60 s did not have any effect on the 5 mM Y^{3+} curve, which indicates that the two-step activation was not a transient behaviour. Concentrations of 10-100 mM Y^{3+} gave a single-step activation of ~200 mV. For these higher concentrations (10 -100 mM) the decrease in overpotential for hydrogen evolution was independent of concentration in the current density range 0.5 A m^{-2} – 10^2 A m^{-2}. The current-density range for activation was however dependent on the Y(III) concentration, a higher Y(III) concentration extending the catalytic effect to a higher current density. Tran *et al.* [40,41] and Hsu and Yen [71] carried out their experiments with $Y(NO_3)_3$ addition to a NaCl electrolyte by starting at open-circuit potential and sweeping towards more cathodic potentials. They explained the lowered overpotential as a catalytic effect on hydrogen evolution caused by yttrium-water complexes formed in the electrolyte bulk, see reaction 27. Water in these complexes was assumed to have a higher reactivity towards reduction, compared to free water molecules, due to weakening of the YOH···H bond.

$$Y(H_2O)_x^{3+} + 3e^- \rightarrow Y(H_2O)_{x-3}^{3+} + \frac{3}{2}H_2 + 3OH^- \qquad (27)$$

Tran *et al.* [40,41] explained the lack of activation at higher current densities as a mass-transport limitation of $Y(H_2O)_x^{3+}$ to the electrode surface. This was supported by the fact that this limitation appeared at higher current density with increasing Y^{3+} concentration. However, according to the yttrium-water-complex hypothesis the degree of activation should increase with increasing $Y(H_2O)_x^{3+}$ concentration. In the nitrate-free and deaerated polarisation curves shown in Figure 18, the activation of the hydrogen evolution reaction is independent of Y^{3+} concentration in the range 10 mM-100 mM Y^{3+}, which implies that the catalytic effect needs another explanation. The suggestion is that the activation relates to the yttrium-water complexes within the film rather than the Y(III)-ion complexes in the bulk. It is likely that the film formed in 1 mM Y(III) electrolyte is thinner than the film formed at higher concentrations. The fact that an Y(III)-ion concentration of 1 mM is not enough to activate the hydrogen evolution reaction implies that the film thickness may be of importance (Figure 18). The lack of activation at higher current densities may, as proposed above, be due to film detachment and hindered re-formation during vigorous hydrogen evolution. Tran *et al.* mentioned that they saw a gradual detachment of the yttrium hydroxide film when the cathodic current was increased above the point at which the activation effect disappeared [40]. If the detachment rate is higher than the re-formation rate no activation would be seen, and since the re-formation rate would be dependent on the Y^{3+} concentration, this might explain why the loss of activation depends on Y^{3+} concentration. However, it is possible that there is a very thin film at high current densities where hydrogen evolution is not activated.

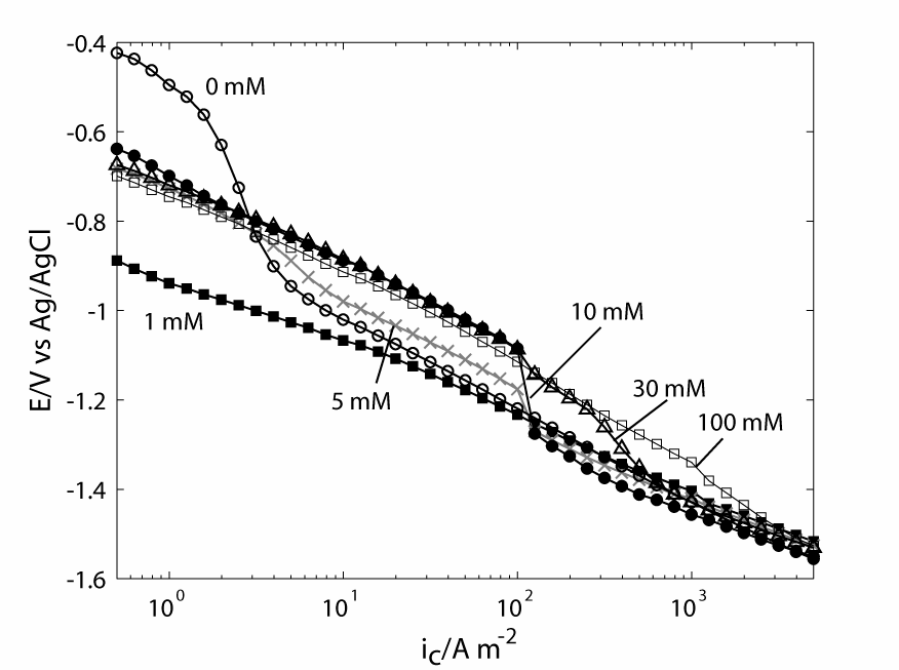

Figure 18. Polarisation curves on iron in electrolytes of different Y^{3+} concentration (0, 1, 5, 10, 30 and 100 mM Y^{3+}). Y^{3+} was added as YCl_3 and the total Cl⁻ concentration, adjusted by NaCl addition, was 0.5 M for all polarisation curves. The polarisation curves were recorded from high to low current densities, i.e. in the anodic direction.

4.5.3 Inhibition of cathodic reactions in presence of Y(III)

The inhibiting effect of REM hydroxide films on oxygen reduction is well known. The results of this study show a hindering of other reactions such as hypochlorite reduction (reaction 12), proton reduction (reaction 21) and nitrate reduction (reaction 28, below) as well when Y(III) is present in the electrolyte.

$$NO_3^- + H_2O + 2e^- \rightarrow NO_2^- + 2OH^- \qquad (28)$$

The effect of yttrium on hypochlorite reduction may be seen in both Figure 17 and 18, where the YCl_3 addition almost completely prevented the reaction. Hypochlorite was generated on the anode while measuring the polarisation curve and the limiting current density for its reduction was easily identified for the yttrium-free electrolyte at ~4 A m^{-2}, when the polarisation curve was recorded from high to low current densities (Figure 17 and 18). Note that a concentration of 1 mM Y(III) was high enough to hinder hypochlorite reduction, whereas it was too low to obtain the catalytic effect on hydrogen evolution, see Figure 18. It is possible that the film formed in electrolyte of low Y(III) concentration is thinner and that a thin film does not exhibit the same catalytic properties as a thicker film.

Figure 19 displays polarisation curves measured in the presence of Y(III) at varying pH values. The limiting current densities for proton reduction, clearly seen in yttrium-free electrolyte in Figure 4, are not seen in the polarisation curves for yttrium-containing electrolyte for pH 3 and 3.5 presented in Figure 19. The electrolyte pH had to be as low as 2.5 before the limiting current density for proton reduction, seen in yttrium-free electrolyte, appeared and then at a current density somewhat lower than for yttrium-free electrolyte. The lack of limiting currents at pH 3 and 3.5 in yttrium-containing electrolyte (Figure 19) indicates the presence of an $Y(OH)_3$ film on the electrode surface, hindering protons and hypochlorite from being reduced. With an Y(III) concentration of 30 mM and a K_{sp} value for reaction 26 of 10^{-22} [69], $Y(OH)_3$ precipitates at pH ~7.2. It may seem remarkable that the yttrium hydroxide film was present even at a bulk pH as low as 3 and at low current densities, when the surface pH most probably was close to the bulk pH. However, this suggests that the yttrium-hydroxide film formed at higher current densities, when the pH close to the electrode surface was high, did not dissolve as the current density was lowered. At a bulk pH lower than 3, the limiting current density for proton reduction appeared as the surface pH became low enough to dissolve the yttrium hydroxide at the electrode surface.

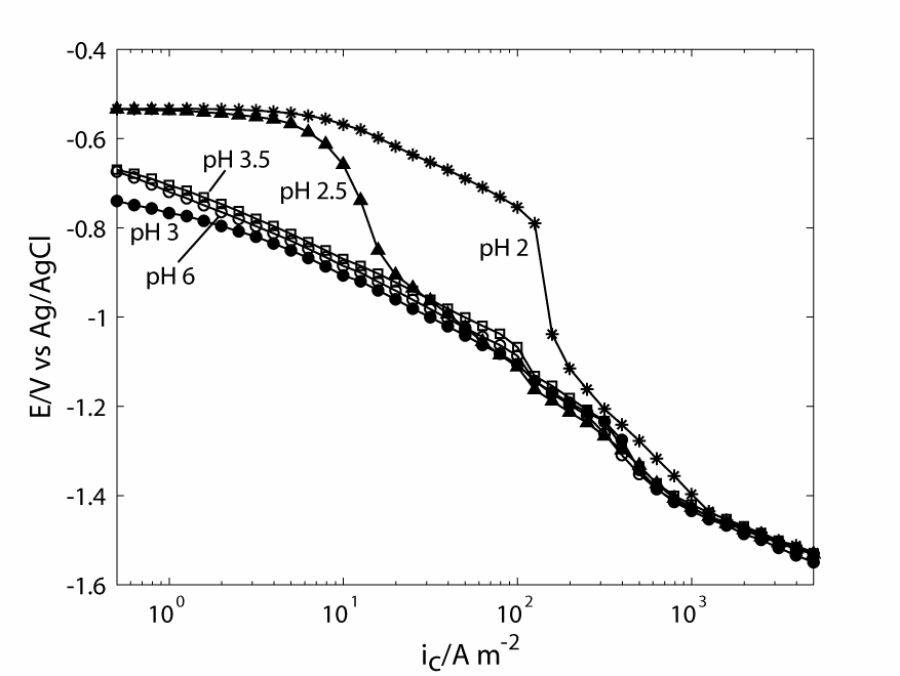

Figure 19. Polarisation curves on iron in NaCl with 30 mM YCl_3, at different pH values. The polarisation curves were recorded in the anodic (←) direction.

Experiments in $NaNO_3$ solution showed that nitrate was reduced on an iron electrode in the absence of Y(III), and that the presence of Y(III) could inhibit nitrate reduction. However, the effect of Y(III) addition on nitrate reduction is more complex than its effect on hypochlorite reduction and proton reduction, and depends highly on the direction the polarisation curve is recorded in. The results of this study show that care must be taken when studying the effect of yttrium on hydrogen evolution in nitrate-containing electrolyte to avoid the impact of nitrate reduction.

4.5.4 Yttrium(III) in chlorate production

The yttrium hydroxide film apparently has the ability to both activate the water reduction and hinder other cathodic reactions. The inhibiting properties are necessary for keeping the high current efficiency for hydrogen evolution when substituting Cr(VI) in the chlorate process. The activating effect would of course be attractive in terms of decreased overpotential and thus decreased energy consumption.

The above experiments were made in 0.5 M NaCl electrolyte, and it had to be investigated whether the addition of Y^{3+} would have the same effect in chlorate electrolyte (550 g/L $NaClO_3$ + 110 g/L NaCl, 70°C). However, it turned out that Y^{3+} precipitated immediately when added to this electrolyte. Lowering the pH dissolved the precipitation. This would however not be an option in the industrial process, since it has to have a pH of around 6-7 to obtain a sufficient rate of chlorate formation (reaction 6).

In the polarisation experiments the RDE was rotated at a speed of 3000 rpm, which gives a considerably higher mass transport than in industrial cells. It was found that a stationary cathode

did not allow the yttrium hydroxide film to form on the surface. Instead yttrium hydroxide precipitated at a distance from the electrode, probably due to the thick diffusion layer of OH^- which increased pH further out from the electrode surface. Mass transport is obviously important for obtaining an yttrium hydroxide film on the cathode.

5. CONCLUSIONS

The objective of this work was to identify possible improvements in chlorate electrolysis, which eventually may reduce the consumption of energy in the chlorate process.

5.1 The critical anode potential

The impact on E_{cr} of different electrolyte parameters was investigated; it was found that E_{cr} depends linearly on the logarithm of chloride concentration at pH 2, with a slope of -90 mV/dec Cl^-. A high chloride concentration is still beneficial in terms of a decreased anode potential, which outweights the negative effect of a decrease in E_{cr}. E_{cr} also decreases with an increased temperature. As in the case of influence of chloride, the negative effect on E_{cr} is compensated by the decreased potential which means that i_{cr} actually increases with increased temperature. Therefore, in terms of adjusting electrolyte parameters the best strategy to avoid exceeding E_{cr} is to try to obtain the lowest possible anode potential.

It is likely that the mechanism for chloride oxidation is the same for potentials below E_{cr} as well as for potentials above E_{cr}. The reason for the higher slope of the polarisation curve could then be a potential-dependent deactivation of the active sites. Deactivation of active ruthenium sites could occur if ruthenium in a higher oxidation state were inactive for chloride oxidation.

In the lab cells used in this work it is relatively easy to measure the anode potential vs a reference electrode and then to note when the potential reaches a certain value, defined as the critical potential. However, in the actual industrial process it is much more complicated to monitor the anode potential. Not only the need for reference electrodes within the cell, but also for instance uneven current distribution and ohmic losses in current collectors and electrolyte makes it very difficult to obtain a reliable value of the potential. A more applicable method is to monitor the oxygen concentration in the cell gas (already done in chlorate plants), as increased oxygen evolution is an indication of the potential exceeding E_{cr}. The current efficiency for chloride oxidation has its maximum at around E_{cr}, which means that it would be desirable to operate the anode at a potential close to but still below E_{cr}. However, an increased concentration of oxygen in the cell gas does not necessarily have to be due to E_{cr} being exceeded, since there are other factors that also affect the evolution of oxygen.

To make the DSA less sensitive to operation at high currents stabilisation of the ruthenium in the DSA would be an option. For instance, iridium-ruthenium based DSAs have shown a higher E_{cr} and a less pronounced bending of the polarisation curve at E_{cr}, than the ruthenium-based DSA [18].

5.2 The impact of buffers

Chlorate electrolyte contains buffering species such as hypochlorite and chromate. When the chlorate process is operated at full load (~3 kA m^{-2}) their buffering capacities do not influence the electrode reactions. However when electricity prices are high and the process is occasionally operated at lower loads they should be considered.

The influence of chromate buffer on oxygen evolution on a DSA (in pure $NaClO_4$ electrolyte) as well as on the cathodic reaction hydrogen evolution on iron (in chlorate electrolyte) was investigated. It was found that the important impact of the chromate buffer was associated with its ability to increase the limiting current densities for OH^- oxidation and H^+ reduction. For oxygen evolution 3 g/L $Na_2Cr_2O_7$ was found to increase the limiting current density for OH^- oxidation by about a decade, but was still far below the current density at full-load operation.

When lowering the load and operating close to the limiting current density only a small current change may cause a large potential step on the cathode as well as on the anode. For a cathode, this may mean that the electrode loses its cathodic protection. For a new steel cathode the potential step was evident, but for corroded steel electrodes H^+ reduction appeared not to take place and thus no potential step was seen. Therefore, when using the old steel electrodes of today´s process, no particular care must be taken in presence of a buffer. However, when using other materials for cathodes the potential step might have to be considered. For the DSA anode the amount of oxygen in the cell gas would most likely increase significantly as the overpotential for oxygen evolution would suddenly decrease at the potential step.

5.3 The cathode overpotential

It was investigated whether it was possible to adjust the electrolyte parameters in order to minimise the cathode overpotential. However, it could be concluded that none of the investigated electrolyte parameters (pH, temperature, mass transport, the concentrations of chloride, chromate and chlorate as well as the presence of hypochlorite) had any major effects on the chlorate cathode potential at full-load current densities, where water reduction was dominating. Although the electrolyte conditions were varied to unrealistic values their impact was never larger than 50 mV, mostly significantly smaller.

Certainly, there is more voltage to gain from changing the cathode material and/or structure than from modifying the electrolyte composition. This is indicated when comparing the results of this study with polarisation measurements on cathodes containing ruthenium, showing considerably lowered overpotentials [72,73]. The importance of the electrode is further shown by the experiments on steel corroded from operation in a chlorate plant, which exhibits significantly higher activity for hydrogen evolution than polished steel or iron. It is likely that the composition at the corroded electrode surface activates the cathode reaction and decreases the overpotential, probably in combination with an increased surface area of the electrode.

5.4 Modelling

A model was developed to illustrate the complex interplay between a pH-dependent electrode reaction (oxygen or hydrogen evolution), mass transport and the buffering due to addition of chromate. It was found that the chromate buffering took place in a thin reaction layer (in the order of nanometers) at the electrode surface. In the reaction layer neither the water dissociation reaction (reaction 18) nor the chromate buffering ($HCrO_4^- + OH^- \leftrightarrow CrO_4^{2-} + H_2O$ or $HCrO_4^- \leftrightarrow CrO_4^{2-} + H^+$) was in equilibrium. The consequence of this is that it is important to have the

reaction rates for these reactions as input data to the model and not to simulate the reactions as if they were in equilibrium. The reaction rates for chromate buffering were not found in the literature, but could be estimated by comparing simulated polarisation curves with experimental curves. It also is important to have a high resolution at the electrode surface to capture the concentration profiles in the very tin reaction layer.

5.5 Activation of hydrogen evolution and inhibition of side reactions by adding Y(III) to the electrolyte

The addition of Y(III) ions to a 0.5 M NaCl electrolyte resulted in the formation of an yttrium hydroxide film on the cathode during hydrogen evolution. It was found that the hydrous, gel-like $Y(OH)_3$ film formed on the iron surface inhibits the reduction of protons, nitrate ions and of hypochlorite ions. At certain conditions the film also catalyses hydrogen evolution from the reduction of water. The reactant of the catalysed water reduction is most likely water molecules coordinated to Y(III) within the yttrium hydroxide film.

Two forms of film may be distinguished. A film formed at conditions expected to favour a relatively thin film, i.e. a low concentration of Y(III) or a high current density when extensive gas evolution disturbs the film formation, hinders the reduction of ions but the film does not activate water reduction. At higher Y(III) concentration and lower current densities the film formed has inhibiting as well as catalytic properties. Loss of activation at high current densities may be a problem in electrolysis applications.

The fact that the film inhibits reduction of hypochlorite while decreasing the overpotential for hydrogen evolution makes yttrium(III) to a promising candidate for replacing chromium(VI) in the chlorate process of today.

Unfortunately, when adding Y(III) to chlorate electrolyte having a higher ionic strength than the electrolyte in this work, yttrium precipitates immediately, most likely as $Y(OH)_3$ in the bulk. Another problem might be the mass transport in industrial cells, which has to be good enough for developing a thin diffusion layer of OH^-. Thicker diffusion layers may lead to precipitation of $Y(OH)_3$ at a distance from the electrode and no film formation on the surface.

Even though yttrium salts may not be used in the chlorate process, this work has supplied new knowledge regarding inhibiting and activating films. It shows that it may be possible to find an alternative to chromate, which besides the inhibiting effects also catalyses hydrogen evolution. Hopefully, with this knowledge alternatives with similar properties, though more suitable for the chlorate process, will be found. These alternatives should have the ability to in a film situ form on the cathode. In the search for a cathode film it may be kept in mind that the thickness of the film and its water content could be factors affecting its catalytic properties.

5.6 Overall conclusions

In this work the role of the electrolyte composition has been investigated in order to minimise the energy consumption. If changing the electrolyte it has to be kept in mind it may cause effects in other stages of the process, and the electrolysis cannot be optimised alone. It turned out that the effect of the electrolyte parameters on the electrode reactions was relatively small, and to minimise the energy consumption to a larger extent the electrode materials should be further looked upon.

The anode overpotential is kept low as long as the DSA contains the active material ruthenium and as long as the critical potential is not exceeded. Although some efforts may be done to decrease the anode potential, so that E_{cr} is not reached, stabilisation of the anode is suggested in case the process occasionally is operated under extreme conditions.

To decrease the cathode overpotential, either a new activated cathode material has to be found or a catalytic film should be applied in-situ on the cathode surface. This work showed that it may be possible to find alternatives to the chromate film used today. It would be interesting to find out whether other metal ions than Y(III) could be added to the electrolyte in order to form hydrous-hydroxides on the cathode, and whether they in that case would both inhibit side reactions and be activating towards hydrogen evolution.

The role of chromate as a buffer is most important for keeping pH in the chlorate cell neutral in order to obtain a high rate of the chlorate forming reaction. The impact on the electrode reactions of a buffer is most likely minor at full load operation. On the cathode, hydrogen is evolved through water reduction, which at high overpotentials is independent of pH. On the anode the chloride oxidation is pH dependent only at very low pH values (below 2) [24]. If the electrolyte pH at the anode surface is that low, chromate might buffer through reaction 17, which perhaps prevents the pH to decrease further. When a substitute for chromate eventually is found it has to be taken into account that the electrolyte has to be buffered to a pH around 6-7.

ACKNOWLEDGEMENTS

I would like to thank Ann Cornell, Mårten Behm and Göran Lindbergh for having been my supervisors, for all the valuable discussions and for encouraging and supporting me.

Thanks to my chlorate colleague John Gustavsson for valuable cooperation during the last one and a half years.

Thanks to the people at Eka Chemicals Technology and Engineering and at Permascand for inspiring me by providing a link between my research and the industrial application.

The meetings with the Electrochemistry group within FaxénLaboratoriet have always been great fun. Thanks to all of you.

To my past and present colleagues at Applied Electrochemistry. I am incredibly happy I have had you as work mates during my years as PhD student.

Speciellt tack till: Andreas N, för våra diskussioner kring artikelskrivande, elektrokemi, teater och livet. Henrik som alltid har tid att lyssna. Tack för dina råd kring modellering och materietransport under de första åren, och tack för allt roligt, bland annat vårt viktiga projekt att besöka och utvärdera Stockholms alla biografer. Tack till mina allra bästa träningskompisar Ivan och Sophie. Ert sällskap får mig att gå iväg till träningen och släppa alla tankar på jobb. Tack Ivan för dina försök att lära mig spurta. Tack Sophie för att du alltid ser när jag behöver muntras upp, för att du bryr dig om så mycket och för att du skapar en glad stämning kring dig. Maria som är den bästa vän man kan tänka sig och som jag även har haft turen att ha som kollega. Förutom din ovärderliga vänskap uppskattar jag alla diskussioner om överpotentialer, reaktionsmekanismer och experimentella lösningar vi haft. Sara, din entusiasm och glädje smittar. Jag ler bara jag tänker på dig! Thanks Shelley for coaching me, correcting my English and trying to teach me freestyle swimming. Och tack Andreas B som alltid är så uppmuntrande, alltid mån om att alla ska må bra.

Tack Andreas. För ditt tålamod, ditt lugn och din oändliga kärlek.

REFERENCES

1. J. E. Coleman, in *Tutorial Lectures in Electrochemical Engineering and Technology*, Vol. 77, R. Alkire and T. Beck, Editors, A.I.Ch.E.Symp. Ser. 204, p. 244, Institute of Chemical Engineers, New York (1981)
2. S. Schlag, K. Yagi, CEH Product Review, *The Chemical Economics Handbook-SRI Consulting* (2005)
3. K. Viswanathan and B. V. Tilak, *J. Electrochem. Soc.*, **131**, 1551 (1984)
4. S. Kotowskii and B. Busse, *Modern Alkali Technology 3*, 310 (1986)
5. K. L. Hardee and L-K. Mitchell, *J. Electrochem. Soc.*, **136**, 3314 (1989)
6. B. V. Tilak and C-P. Chen, in *Chlor-Alkali and Chlorate Technology*, H. S. Burney, N. Furuya, F. Hine, and K. I. Ota, Editors, PV 99-21, p. 8, The Electrochemical Society Proceedings Series, Pennington, NJ (1999)
7. J.P. Hoare, *Electrochemistry of Oxygen*, Interscience Publishers, USA (1968)
8. S. Trasatti, in J. Lipkowski, P.N. Ross (Eds.), *Electrochemistry of Novel Materials*, VCH, New York (1994)
9. N. Sato and G. Okamoto, *Electrochim. Acta*, **10**, 465 (1965)
10. A. Cornell, G. Lindbergh and D. Simonsson, *Electrochim. Acta*, **37**, 1873 (1992)
11. B. V. Tilak, K. Tari and C. L. Hoover, *J. Electrochem. Soc.*, **135**, 1386 (1988)
12. F. Hine and M. Yasuda, *J. Electrochem. Soc.*, **118**, 182 (1971)
13. G. Lindbergh and D. Simonsson, *J. Electrochem. Soc.*, **137**, 3094 (1990)
14. G. Lindbergh and D. Simonsson, *Electrochim. Acta*, **36**, 1985 (1991)
15. A. Ahlberg Tidblad and G. Lindbergh, *Electrochim. Acta*, **36**, 1605 (1991)
16. V. I. Eberil, N. S. Fedotova and E. A. Novikov, *Elektrokhimiya*, **33**, 610 (1997)
17. A. Cornell, B. Håkansson and G. Lindbergh, *J. Electrochem. Soc.*, **150**, D6 (2003)
18. V. I. Eberil, N. S. Fedotova and E. A. Novikov, *Elektrokhimiya*, **33**, 713 (1997)
19. F. A. Cotton and G. Wilkinson, in *Advanced Inorganic Chemistry 5th ed.*, John Wiley & Sons, New York (1988)
20. J. G. Mason and A. D. Kowalak, *Inorg. Chem.*, **3**, 1248 (1964)
21. J. D. Neuss and W. Riemann III, *J. Am. Chem. Soc.*, **56**, 2238 (1934)
22. P. Byrne, E. Fontes, O. Parhammar and G. Lindbergh, *J. Electrochem. Soc.*, **148**, D125 (2001)
23. J. L. Fernández, M. R. Gennero de Chialvio and A. C. Chialvio, *Electrochim. Acta*, **47**, 1129 (2002)
24. S. Trasatti, *Modern Chlor-Alkali Tech.*, Vol 6, R. W. Curry, Editor, The Royal Society of Chemistry, p. 110, London (1995)
25. V. I. Eberil, N. S. Fedotova, E. A. Novikov and A. F. Mazanko, *Elektrokhimiya*, **36**, 1463 (2000)
26. J. Wulff and A. Cornell, *J. Appl. Electrochem.*, **37**, 181 (2007)
27. N. Ibl and H. Vogt, in J. O´M Bockris, B.E. Conway, E. Yeager and R.E. White (ed) *Comprehensive Treatise of Electrochemistry*, Vol. 2, , p. 167, Plenum Press, New York (1981)
28. M. M. Jaksic, *J. Electrochem. Soc.* **121**, 70 (1974)

29. L. Hammar and G. Wranglén, *Electrochim. Acta*, **9**, 1 (1964)
30. A. Cornell, B. Håkansson and G. Lindbergh, *Electrochim. Acta*, **48**, 473 (2003)
31. L. M. Elina, V. M. Gitneva, V. I. Bystrov and N. M. Shmygul, *Elektrokhimiya*, **10**, 68 (1974)
32. M. M. Jaksic, B. Z. Nikolic, D. M. Karanovic and C. R. Milovanovic, *J. Electrochem. Soc.*, **116**, 394 (1969)
33. Yu. V. Dobrov and L. M. Elina, *Zashchita Metallov*, **3**, 618 (1967)
34. F. Andolfatto, P. Joubert and G. Duboeuff, FR 2852973 (2004)
35. D. Guay, L. Roue, R. Schulz and M-E. Bonneau, CA 2492128 (2006)
36. N. Chow, J. Socol, K. Oehr and G. Rempel, WO 2006039804
37. N. Krstajic, V. Jovic and G. N. Martelli, WO 2007063081 (2007)
38. J. R. Jackson and M. Zhao, US 2005011753 (2005)
39. B. Håkansson, E. Fontes, F. Herlitz and V. Lindstrand, US 2004124094 (2004)
40. M. Tran, C. Fiaud and E. M. M. Sutter, *J. Electrochem. Soc.*, **153**, B83 (2006)
41. M. Tran, D. Mohammedi, C. Faud and E. M. M. Sutter, *Corros. Sci.*, **48**, 4257 (2006)
42. M. Bethencourt, F. J. Botana, J. J. Calvino, M. Marcos and M. A. Rodríguez-Chacón, *Corros. Sci.*, **40**, 1803 (1998)
43. S. Bernal, F. J. Botana, J. J. Calvino, M. Marcos, J. A. Pérez-Omil and H. Vidal, *J. Alloys Compd.*, **225**, 638 (1995)
44. B. R. W. Hinton, *J. Alloys Compd.*, **180**, 15 (1992)
45. K. Aramaki, *Corros. Sci.*, **43**, 1573 (2001)
46. M. F. Montemor, A. M. Simões and M. G. S. Feirreira, *Progr. Org. Coat.*, **44**, 111 (2002)
47. C. T. Hsu and S. K. Yen, *J. Electrochem. Soc.*, **152**, C813 (2005)
48. H. B. Beer, *J. Electrochem. Soc.*, **127**, C303 (1980)
49. T. Loucka, *J. Appl. Electrochem.*, **20**, 522 (1990)
50. R. Kötz, H. J. Lewerenz and S. Stucki, *J. Electrochem. Soc.*, **130**, 825 (1983)
51. A. C. Riddiford, in *Advances in Electrochemistry and Electrochemical Engineering*, Vol. 4, p. 61, John Wiley & Sons, New York (1966)
52. M. Stern, *J. Electrochem. Soc.*, **102**, 609 (1955)
53. J. Albery, in *Electrode Kinetics*, p. 125, Clarendon Press, Oxford (1975)
54. M. M. Jaksic, A. R. Despic, B. Z. Nikoloc and S. M. Maksic, *Croatica Chemica Acta*, **44**, 61 (1972)
55. B. K. S. Rao and M. Sharma, *Bull. Electrochem.*, **6**, 773 (1990)
56. B. V. Tilak, K. Viswanathan and C. G. Rader, *J. Electrochem. Soc.*, **126**, 1228 (1981)
57. L. C. Adam, I. Fábián, K. Suzuki and G. Gordon, *Inorg. Chem.* **31**, 3534 (1992)
58. T. Hurlen, S. Gunvaldsen and F. Blaker, *Electrochim. Acta*, **29**, 1163 (1984)
59. W. J. Moore, *Basic Physical Chemistry*, Prentice-Hall International, 1983, p. 293
60. A. Cornell, *PhD Thesis*, Royal Institute of Technology KTH, Stockholm (2002)
61. S. Trasatti, *Electrochim. Acta*, **36**, 225 (1991)
62. D. V. Kokoulina, Yu. I. Krasovitskaya and T. V. Ivanova, *Elektrokhimiya*, **14**, 470 (1978)
63. M. H. Miles, E. A. Klaus, B. P. Gunn, J. R. Locker and W. E. Serafin, *Electrochim. Acta*, **23**, 521 (1978)
64. S. Jin, S. Ye, *Electrochim. Acta*, **41(6)**, 827 (1996)

65. L.I. Krishtalik, *Electrochim. Acta*, **26**, 329 (1981)
66. L. D. Burke, O. J. Murphy, J.F. O'Neill and S. Venkatesan, *J. Chem. Soc. Faraday Trans. 1*, **73**, 1659 (1977)
67. S. Trasatti, *Electrochim. Acta*, **32**, 369 (1987)
68. A. Ahlberg Tidblad and J. Mårtensson, *Electrochim. Acta*, **42**, 389 (1997)
69. D. R. Lide, ed., *CRC Handbook of Chemistry and Physics 88th ed*, CRC Press, p. 8-118 (2007-2008), http://www.hbcpnetbase.com/ accessed 01/02/2008
70. M. Pourbaix, in *Atlas of Electrochemical Equlibria in Aqueous Solutions*, p. 181, Pergamon Press, London (1966)
71. C. T. Hsu and S. K. Yen, *J. Electrochem. Soc.*, **152**, C813 (2005)
72. S. Jin, A. Van Neste, E. Ghali, S. Boily and R. Schultz, *J. Electrochem. Soc.*, **144**, 4272 (1997)
73. A. Cornell and D. Simonsson, *J. Electrochem. Soc.*, **140**, 3123 (1993)